

Out-of-Plane Loaded Masonry Walls Retrofitted with Oriented Strand Boards: Numerical Analysis and Influencing Parameters

Jamiu A. Dauda^{a,b}, Luis C. Silva^c, Paulo B. Lourenço^d and Ornella Iuorio^b

^aSchool of Architecture, Built and Env., University of Wales Trinity Saint David, SA1 8EW, Swansea, UK.

^bSchool of Civil Engineering, University of Leeds, Woodhouse Lane, LS2 9JT, Leeds, United Kingdom.

E-mail: j.dauda@uwtsd.ac.uk; o.iuorio@leeds.ac.uk

^cFaculty of Engineering, University Lusófona de Humanidades e Tecnologia, Lisbon, Portugal.

Email: luis.silva@ulusofona.pt

^dISISE, University of Minho, Azurém, 4800-058 Guimarães, Portugal.

Email: pbl@civil.uminho.pt

HIGHLIGHTS

- Numerical modelling of a masonry wall retrofitted using oriented strand board and anchor rods.
- The numerical model predicted the experimental data within a 10% deviation.
- The influence of the OSB thickness, position, and anchor rods spacing was studied.
- An increase in OSB thickness leads to higher efficacy of the proposed retrofit system.
- The study recommends 250 - 500mm spacing between anchor rods for better efficiency.

ABSTRACT

The computational prediction of the out-of-plane behaviour of unreinforced masonry walls is a challenge. However, computational numerical models, if properly calibrated, may provide a powerful tool to predict the behaviour of new retrofit techniques with negligible effort. This paper presents high accuracy Finite Element (FE) modelling for the prediction of out-of-plane behaviour of masonry walls retrofitted with oriented strand boards (OSB). This retrofit measure has been proposed by the authors for brick masonry walls and its efficiency has been demonstrated through experimental studies on small-scale and larger-scale masonry specimens (out-of-plane monotonic tests). The data gathered in the experimental phase has been used to calibrate numerical FE-based models (i.e. non-retrofitted and retrofitted) presented in this paper. For this purpose, a detailed micro-modelling strategy has been followed assuming a perfect bond between mortar joints and brick units. The so-called Concrete Damage Plasticity (CDP) model has been adopted to describe the constitutive relation of the masonry and the OSB timber panel. The connection between the masonry and OSB panel has been modelled through elastic anchors. The numerical results show a good agreement with the experimental data, in terms of observed damage pattern and capacity curve (within 10% difference). The calibrated numerical model has been instrumental in developing a parametric analysis to study the effect of different OSB thicknesses, the side of the application of retrofit, and the spacing between connections through anchor rods. These revealed that the out-of-plane capacity of the system is directly proportional to the OSB thickness and that the spacing between steel connectors should be lower than 500mm for an adequate response.

KEYWORDS

Capacity Curve, Concrete Damage Plasticity, Numerical Analysis, Oriented Strand Board, Out-of-Plane, Retrofitting Masonry Wall.

1 INTRODUCTION

Masonry is one of the oldest construction materials, but it is also one of the more complex when assessing its mechanical properties and its structural behaviour [1]. High uncertainty related to its mechanical behaviour and the intrinsic heterogeneity due to the arrangement of masonry components turns the structural response of such buildings a complex and hard to predict task [2], [3], and [4]. The main difficulty is typically attributed to the presence of mortar joints that act as planes of weakness, hence creating non-linear discontinuities within the composite material. Thus, the uncertainties related to the mechanical and geometrical properties can strongly affect the analysis of masonry structures [5–7].

Owing to these difficulties and through a logical extension, the evaluation of the mechanical response of a retrofitted masonry wall is also complex. Structural retrofitting is a process that aims to generally improve the structural capacity and ductility of existing buildings [8]. In the case of URM walls, retrofits are used to offer some structural capacity upgrade or structural damage control [9]. Some of the existing retrofit techniques used in masonry walls include joint treatment such as repointing and grout injection; surface treatment such as textile-reinforced mortars coating and reinforced plaster; and FRP wrapping (the reader is referred to [10] and [11] for an extensive review of existing retrofit techniques). In this study, the application of oriented strand board (OSB) type 3 panel to retrofit URM walls is proposed [12]. OSB type 3 is a load bearing engineered wood-based panel for use in humid conditions. OSB is regarded as a promising wood-based structural panel due to its superior strength, stiffness, workability, and competitive pricing [13]. The main advantages of timber-based retrofit solutions are related to low cost and sustainability. Few experimental studies such as [14], [15], and [16] investigated the application of timber panels as a strengthening system for existing masonry buildings. Since the mode-I type of failure (i.e. tensile failure associated with stresses acting normal to joints and leading to the separation of the interface) is the most common in masonry structures [17], out-of-plane tests are typically considered to study the effectiveness of a retrofit technique against flexural failure of masonry walls [18], [19], [20], [21] and [22].

However, experimental tests may be expensive and time-consuming. In such a context, computational numerical analyses are useful and convenient to provide an efficient alternative to full-scale testing of out-of-plane strength of retrofitted masonry walls. Computational numerical models, if properly calibrated can predict the behaviour of masonry walls subjected to a given applied load. These may be based on different theories, such as the finite element method (FEM), discrete/distinct element methods (DEM), or particle flow code (PFC), among others [23], [24], and [25]. FEM-based models are the most widely used for the case of masonry structures and within different modelling strategies i.e. (i) detailed micro-modelling strategy, (ii) simplified micro-modelling strategy, and (iii) macro-modelling strategy [2], [26], [27], [28] and [29].

The detailed micro-modelling strategy represents the masonry arrangement without any simplification over its geometrical configuration. Hence, masonry units and mortar joints are represented by continuum FEs (finite elements) while the unit-mortar interface can be represented by interface FEs [23] or, in the limit, being disregarded if a perfect bond is assumed. Although this assumption may provide the most accurate results, it also requires an intensive computational time due to the detailed level of refinement (see [7] and [30]). In the simplified micro-modelling strategy, masonry units are represented as fictitious expanded units, and through continuum FEs; the size of units is given by their original dimensions plus the real thickness of mortar joints. Therefore, mortar joints are modelled as zero-thickness interface FEs. This simplification leads to the reduction of the computational effort and yields a model that applies to a wider range of structures. On the other hand, macro-modelling is a strategy oriented for structural level analysis, whereas masonry is modelled as one phase material by smearing out masonry units, mortar, and unit-mortar interface in an equivalent homogeneous

material. This method has been previously adopted by [31], [32], [33] and [34]. The macro-modelling procedure is preferred for analysis of large-scale structures but may neglect some failure modes given by local damage (high stress-gradients).

The choice over the type of modelling depends on the amount (and quality) of the material information available and the level of accuracy and simplicity desired ([9], [35]). Macro-modelling is the most practical-oriented FE strategy since it requires lower computational times and memory allocation. It also allows a faster pre-processing stage since it is easier to model and mesh the structural component or structure [23]. This type of modelling is valuable when a compromise between accuracy and efficiency is needed. On the other hand, micro-models produce the most accurate results but are computationally intensive due to the required precise level of refinement. A convenient guideline aiming to ease the selection of the indicated FE modelling type in the case of historical masonry structures is given in [24].

In this study, a detailed micro-modelling strategy with the unit-joint interface precluded is adopted, meaning that a perfect bond (merged interface nodes) is assumed. Such a decision is supported by experimental data at disposal [24]. The experimental tests analysed correspond to a flexural bond strength test on a $665 \times 215 \times 102.5 \text{ mm}^3$ masonry prism [36] and an out-of-plane loading test on a $1115 \times 1115 \times 215 \text{ mm}^3$ masonry wall [37]. A brief overview of the experimental works carried out at the George Earle Lab at the University of Leeds is provided in section 2. Thus, an FE model has been developed and calibrated considering the previous experimental campaigns reported in [36] and [37]. The main objective of this paper is to develop a calibrated ad-hoc numerical model that can further enrich, through a parametric analysis, the data collected from the experimental campaign and provide relevant conclusions for the application of the retrofit solution. The numerical calibration includes nonlinear three-dimensional analysis and details the mechanical response of the masonry experiments in terms of obtained damage, failure pattern, and capacity curves for both the non-retrofitted and retrofitted cases. Section 3 presents in detail the numerical study including the model development, validation, and type of analysis performed. Section 4 provides a comparison and discussion between the numerical and experimental results. The calibrated numerical model is then employed to evaluate the performance of the proposed OSB retrofit techniques for the case of masonry walls with different panels and connection configurations; allowing to explore the fundamental advantage of numerical models. In this regard, a parametric analysis is performed to assess the model capability to simulate URM walls retrofitted with different OSB panel thickness, different spacings between connections, and different positions for the retrofit application (Section 5). Remarks and recommendations for future studies are given in section 6.

2 EXPERIMENTAL CASE STUDY

The experimental case study comprises a masonry prism (MP) specimen tested for flexural bond strength [36] and a masonry wall specimen tested under out-of-plane loading [37]. The latter experimental tests were grouped as small-scale and larger-scale tests, respectively, and such designations are adopted hereafter. The studied masonry follows an English-bond arrangement, which is the oldest and more popular form of brick bond in the United Kingdom [38]. For such exploratory work, a monotonic loading was assumed, as it is simpler to implement in the laboratory when compared to a cyclic one. Furthermore, even if related to other retrofitting techniques, some studies proved that monotonic tests provide representative information and are good indicators of seismic behaviour. For instance, Yasser and Robert [53] concluded that these are appropriate to study the seismic resistance of masonry walls retrofitted with fibre-reinforced polymers, as similar failure modes and strength values were found with those obtained from cyclic loading. Griffith et al.

[54] observed similar conclusions, as cyclic loading was found to have a minimal effect on the flexural strength of masonry walls retrofitted with near-surface-mounted carbon fibre polymer.

2.1 Small-scale tests

Small-scale tests on $215 \times 102.5 \times 665 \text{ mm}^3$ masonry prisms (MP) were constructed. Brick units have dimensions of $215 \times 102.5 \times 65 \text{ mm}^3$ and mortar joints of 10 mm thickness. For the retrofitted MP, an 18mm thick OSB board was connected using $\varnothing 8 \text{ mm}/L50 \text{ mm}$ (diameter/length) threaded anchor rods together with injection mortar [36]. The out-of-plane capacity of the MPs for vertical bending was obtained from four-point bending tests ([39], [40]), as given in Figure 1. At the bottom, a roller support was placed to allow it to freely rotate around its base while deflecting out-of-plane. Therefore, although the masonry prism is vertically placed, the tests were conducted under simply supported boundary conditions and without a vertical pre-compression load.

The purpose of this test was to gather data on the flexural strength of plain MP and retrofitted MP (with 18mm thick OSB timber panel) and, therefore, to provide an insight into the effectiveness of the OSB panel in terms of the flexural behaviour improvement. A total of four linear variable displacement transducers (LVDTs) were placed to record the deflections of the test specimen along the centre, mid-top and bottom of the wall. The test was conducted in load control, in which the loading scheme was such that an initial load of 200N increments at every two minutes up to the occurrence of first cracks was applied. Thereafter, there was a continuous loading increment up to the cracking of the MP specimens. The reader is referred to [36] for further details.

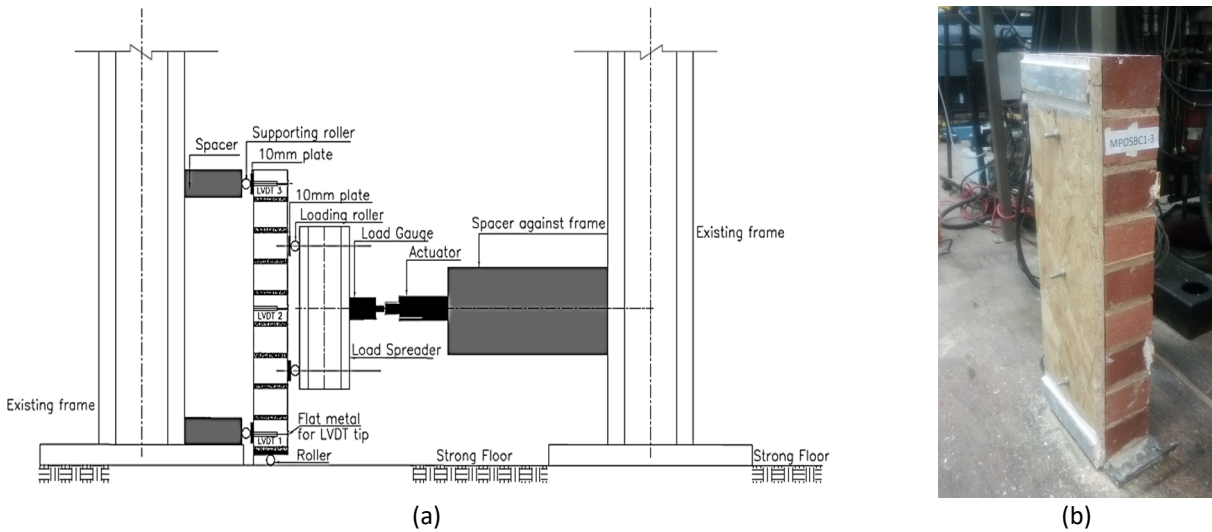


Figure 1. The (a) setup for the small-scale masonry prisms (MPs), and (b) presentation of a retrofitted (with an OSB panel) MP.

2.2 Larger-scale tests

Larger-scale tests were performed on walls ($1115 \times 1115 \times 215 \text{ mm}^3$) with single and double wythes. Mortar joints have a 10mm thickness. The larger-scale test involved performing out-of-plane load control tests on six masonry wall specimens including plain walls, single-sided retrofitted samples, and double-sided retrofitted samples (see Figure 2b-d). A brief discussion of the large-scale experimental setup is presented as follows. Again, the reader is referred to [37] for a detailed discussion of the larger-scale experimental works.

The general test setup (see Figure 2a) was designed to replicate a four-point loading test arrangement aiming at the assessment of the out-of-plane behaviour of the masonry wall. Each wall specimen was tested by

applying an out-of-plane monotonic load, as it has been studied by other studies when assessing the efficiency of a retrofit technique [20] and [21]. The specimens were tested with simply supported boundary conditions and with vertical pre-compression stress on top of the walls of 0.05 MPa, as presented in Figure 2a.

The simply supported boundary condition of the specimen was achieved by supporting the back of the wall across the middle of the top and bottom course with backing steel frames. The backing frames were connected to an existing stanchion as a reaction frame at the top and bottom of the wall. A 25mm diameter roller was placed between the back face of the wall and the supporting steel plate on the reaction frames to provide for smooth distribution of load action across the length of the wall and avoid point contact. Once the setup was completed, a 50mm diameter roller was inserted under the specimen. This allowed the wall to freely rotate around its base while deflecting out-of-plane and preventing any restrained end condition.

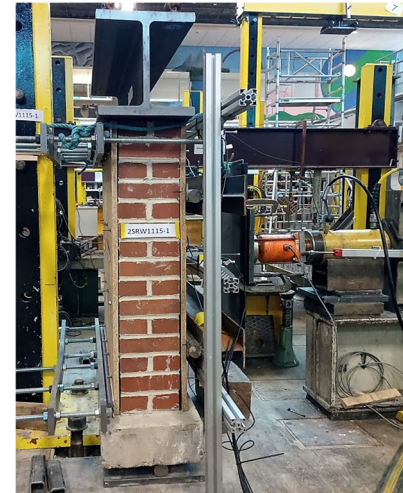
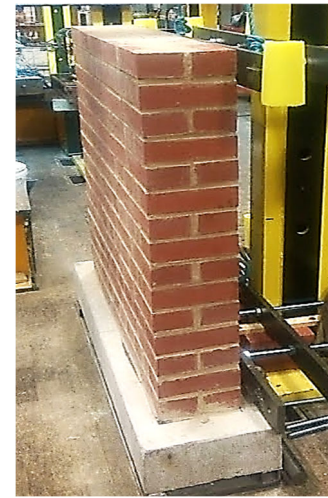
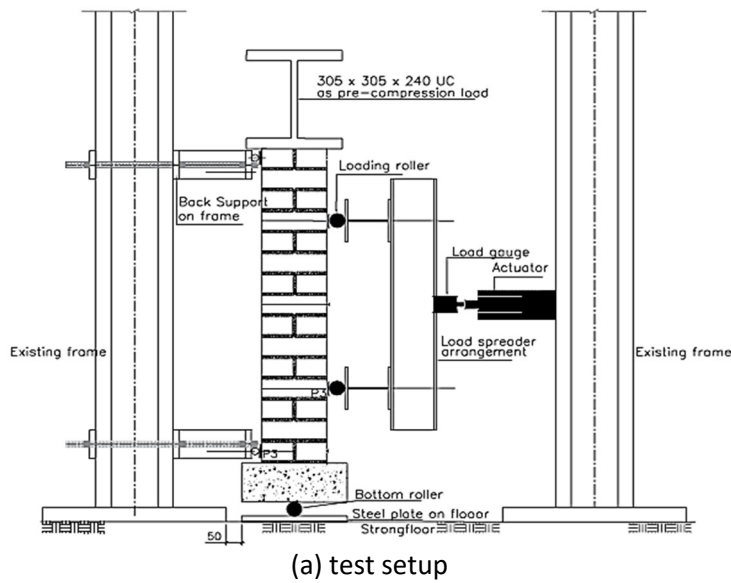


Figure 2. Description of the larger-scale masonry walls tested.

3 NUMERICAL FE-BASED PROCEDURE

A numerical analysis based on the Finite Element Method was performed aiming to extend the experimental works and, therefore, to give further insights on the evaluation of the proposed timber-based retrofit efficiency for URM walls. The commercial software Abaqus/CAE [41] was adopted for the numerical analyses.

The performed study was articulated in two main stages, in analogy with the experimental campaign presented in section 2. It is important to address that material characterization tests, through masonry compression tests on masonry cubic specimens ($215 \times 215 \times 215 \text{ mm}^3$) together with numerical analyses, were conducted and given in [42] and [43]. The main outcome of such studies was to derive paramount information on the material properties to be used herein. Specifically, the density, the Poisson ratio, Young's modulus, and the compressive strength values for both the masonry components (brick units and mortar joints). These materials properties were used herein for the two main stages of the numerical study, being the spatial variability disregarded.

The first stage of the analysis includes the numerical simulation of the flexural bond strength test of the small-scale MPs ($665 \times 215 \times 102.5 \text{ mm}^3$). Here, the numerical FE model is needed to capture the reported damage and failure patterns. This stage was done in two steps; (i) validation of the plain MP using the calibrated properties (of the first stage) for brick units and mortar joints; and (ii) calibration of the retrofitted MPs. For the latter, the properties of the OSB panel and the associated connections were calibrated, and details are given in section 3.1.2.

The second stage of the analysis involves the numerical simulation of the out-of-plane loading test on the larger-scale masonry wall ($1115 \times 1115 \times 215 \text{ mm}^3$). The numerical analysis of this larger-scale masonry wall follows the small-scale model, and both the non-retrofitted and retrofitted models are considered. Finally, a parametric analysis was carried out to assess the model capability to simulate URM walls retrofitted with OSB panels with different thicknesses, different sides for the application, and different connection layouts.

3.1 Modelling description

Two different models were developed for the plain and retrofitted small-scale masonry prisms and were designated, respectively, as MP00-NM and MPOSB-NM. Such terminology follows the one given in the experimental campaign, i.e., MP00 for plain MP and MPOSB for OSB retrofitted MP. Note that NM at the end refers to 'numerical model'. In the same vein, three different models were created for the larger-scale masonry wall, namely, for the plain wall (PW1115-NM), one side retrofitted masonry wall (1SRW1115-NM), and two sides retrofitted masonry wall (2SRW1115-NM). A detailed micro-modelling strategy was followed, in which the unit-joint interface was precluded and, therefore, a perfect bond was assumed. Hence the mesh nodes of the interface were merged. Such a decision is supported by data at disposal concerning the experimental tests performed by the authors [24] and especially well posed for weak mortar masonries [44], as damage tends to be governed by mortar joints, as it is the one being investigated. Solid FEs were used for the modelling of both non-retrofitted and retrofitted masonry models.

3.1.1 Non-retrofitted masonry models

The plain masonry prism (MP00-NM) and plain wall (PW1115-NM) models comprise three components: brick units, mortar joints, and steel plates for loading and support application. Each of these components was modelled as a separate part and assembled as shown in Figure 3. Brick units and mortar joints were modelled as deformable 8-node linear brick FEs (C3D8R) with reduced integration and hourglass control for improved convergence. Steel plate elements for the application of the loading and support conditions were modelled using three-dimensional rigid elements, hence discretized (R3D4) to represent a part that is stiffer than the masonry prism to the point that the deformation is negligible.

3.1.2 Retrofitted masonry models

The numerical models for the retrofitted MP (MPOSB-NM) and the wall (1SRW1115-NM and 2SRW1115-NM) were developed with the addition of two new parts to the plain models. The two additional parts, which are the OSB timber panel, and the anchor rod were modelled as three-dimensional deformable parts and meshed with a hexahedral 8-node linear brick (C3D8R) (see Figure 4). To replicate the retrofit application in the model, the brick unit and OSB timber panel were cut out in the locations where the anchor rods of $\varnothing 8\text{mm}/\text{L}50\text{mm}$ (diameter/length) were used in the experiment [36]. The cut out in the masonry wall and OSB timber panel indicates the anchor rod holes, which allows the model to capture the interaction between the perimeter of the anchor rods and the holes. This represents a rigorous model, with a high level of detail, that should allow achieving accurate results.

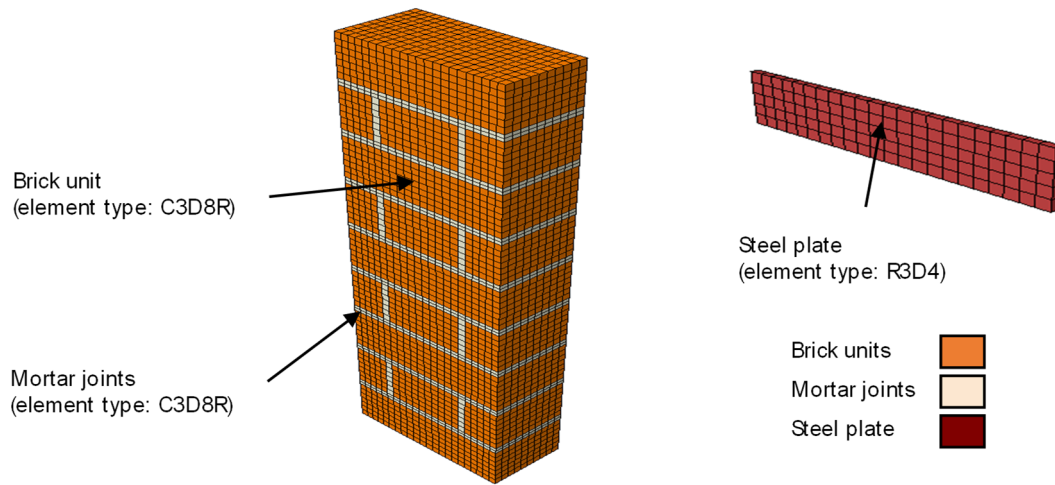


Figure 3. Schematic representation of the non-retrofitted numerical model for the masonry prisms (MP).

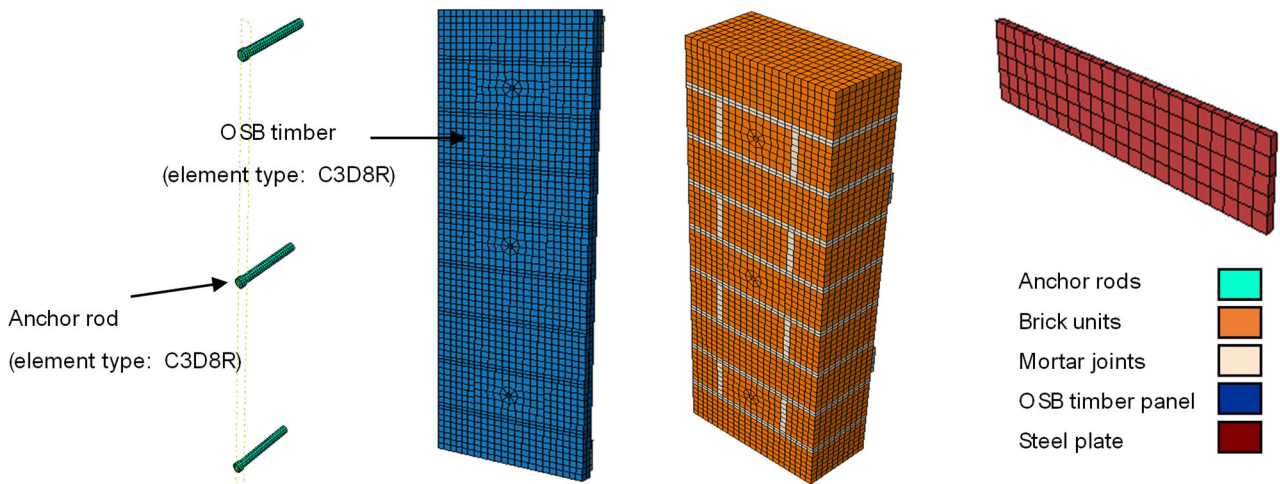


Figure 4. Schematic representation of the retrofitted numerical model: (a) anchor rod; (b) OSB timber; (c) masonry prism (MP) model; and (d) steel plate.

At last, although not presented here, the influence of the FE mesh size was investigated [43][43]. A general well-structured and refined mesh size of 10mm was assumed for the solid FEs. It was found to give accurate results and to avoid convergence issues. The latter mesh size was generally attributed for the modelling of brick units, mortar joints, OSB panel, and steel plates. It should be pointed out, however, that a more refined

FE discretization was used in several regions of the model. For instance, an approximate mesh size of 5mm was adopted for mortar bed joints and a mesh size of 3mm was adopted for brick units in the vicinity of anchor holes. Here, the FE mesh size is especially important to cope with convergence issues. Therefore, the edges of the anchors were also seeded to fulfil the same number of elements around the holes within brick units (i.e. number of element sizing control mesh).

3.2 Interaction and constraint conditions

The numerical model requires interactions and constraint conditions to be implemented that may properly represent the contact relationship between each component of the model: (i) connection between brick units and mortar joints; (ii) connection between brick units and steel plates; (iii) the connection between the steel plates and the OSB panel (for the retrofitted model only); and the (iv) connection between the anchor rods and brick units (for the retrofitted model only). A perfect bond or connection between the brick units' continuum FEs and the mortar joints' FE was assumed, as shown in Figure 5a. Hence the brick-mortar bond interface has not been explicitly represented and the nodes were merged. To what concerns steel plate connections, as given in Figure 5b, the front face surface of the steel plate was tied to the outer surface of brick units using tie constraints. A similar constraint was adopted for the modelling of the connection between the steel plates that serve as support and the masonry connection (see Figure 5c). The use of tie constraints ensures that slip occurrence between steel plates and correspondent brick units is precluded during the analysis.

In the retrofitted model, the back-steel plates were tied to the back of the OSB panel (Figure 5d). Frictional and a normal hard contact were assumed, meaning that no penetration occurs between the OSB timber and MP model, as shown in Figure 5e. In this interaction, the friction coefficient was taken as 0.5, which corresponds to a typical coefficient of friction given between timber and brick surfaces [45]. The connection between anchor rods and brick units, within the anchorage holes, was defined by a surface-to-surface contact method (Figure 5f). Normal and cohesive behaviours were characterized. In the former, a default contact enforcement was defined, meaning that the software sets the penalty stiffness to be ten times higher than the representative underlying element stiffness. In the latter, the cohesive behaviour was also defined through default traction-separation relationships given in ABAQUS. Although it is important to evaluate the response of such interfaces, as pointed out by Park et al. [46], convergence issues related to non-physical responses were not found, at least for the present application. The final assemblage of both the plain and retrofitted models is given in Figure 6.

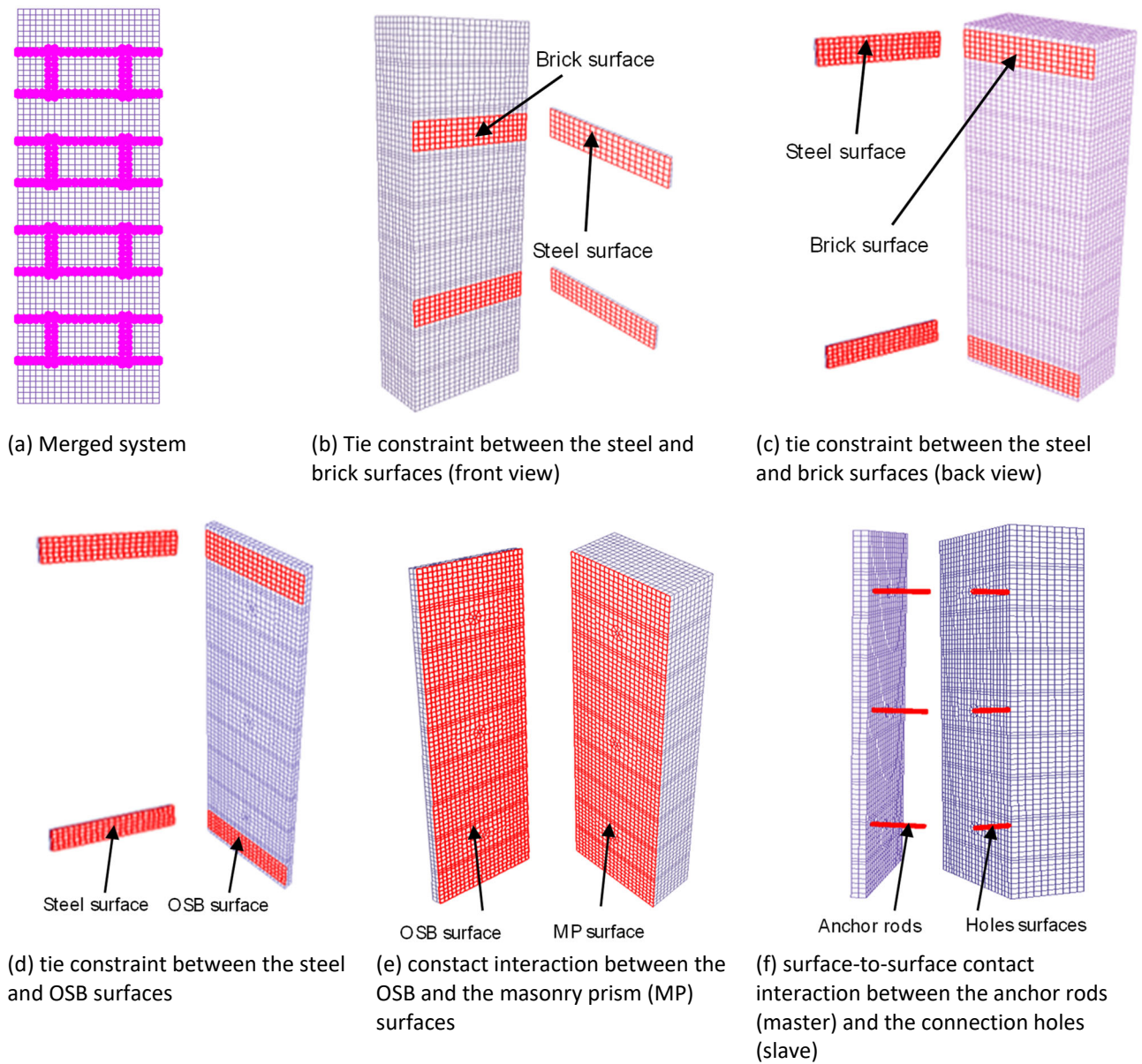


Figure 5. Constraints and interaction surfaces in MP model.

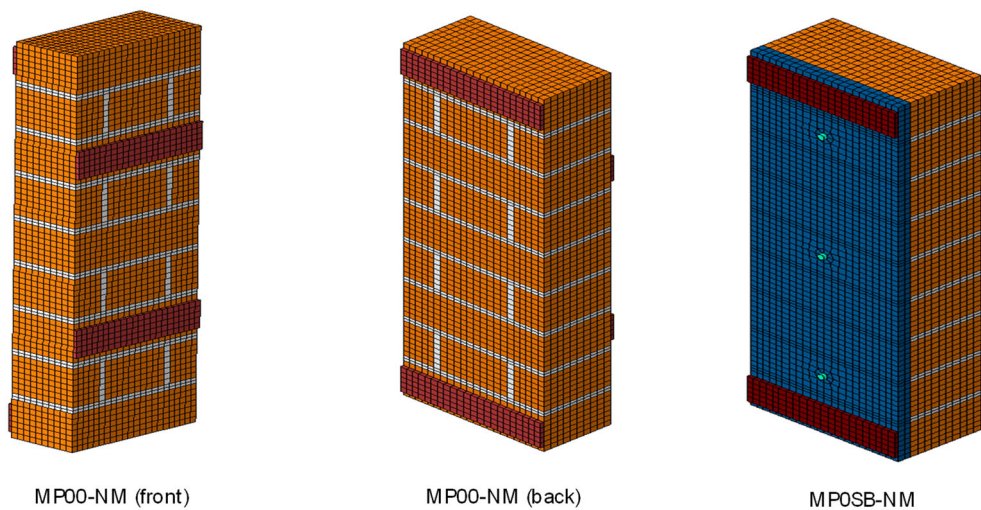


Figure 6. Numerical FE model for both the non-strengthened and strengthened masonry prisms.

3.3 Boundary conditions and loading

Boundary conditions have a critical role in the response of masonry walls under out-of-plane loading (as addressed in [35] and [47]). As such, the numerical models were constrained following the reference experimental tests that serve as calibration, see Figure 1a and Figure 2a. Masonry prisms (MP) were modelled as being simply supported in the centre of the attached steel plates (Figure 7a). The loading on the small-scale MP models includes the self-weight and a unitary out-of-plane surface load placed at the steel loading plates, as indicated in Figure 7b. Again, such loading and support arrangement tries to replicate the four-point bending test carried out in the laboratory [36]. Also, Figure 8 shows the general arrangement, the boundary conditions, and the applied load of the larger-scale masonry wall models. Note that only half of the four-point loading test arrangement was modelled due to symmetry conditions. For this reason, symmetric boundary conditions were defined, i.e., fixed translation in z-axis and rotations around the x- and y-axes (see Figure 8). It is also important to remark that the roller supports applied at the bottom face of the masonry walls are especially important from an experimental standpoint, i.e., to possibly simply supported conditions for the wall, hence disregarded in the numerical models.

Thereafter, the full behaviour of masonry prism and wall model under a continuous increase of load in the form of load-displacement was obtained using the static RIKS method, commonly referred to as the arc-length control method. The quasi-static numerical analyses were conducted through load control alike to the test condition. In the analysis, the load is proportionally applied in several load steps. The equilibrium iteration is performed at each load increment, and the equilibrium path is tracked in the load-displacement space. This method is a robust method for nonlinear analysis, and it can embed the material damage property in the model. After performing the analysis, the damage pattern of the developed numerical model in terms of compressive damage (DAMAGEC) and tensile damage (DAMAGET) were also obtained from the model.

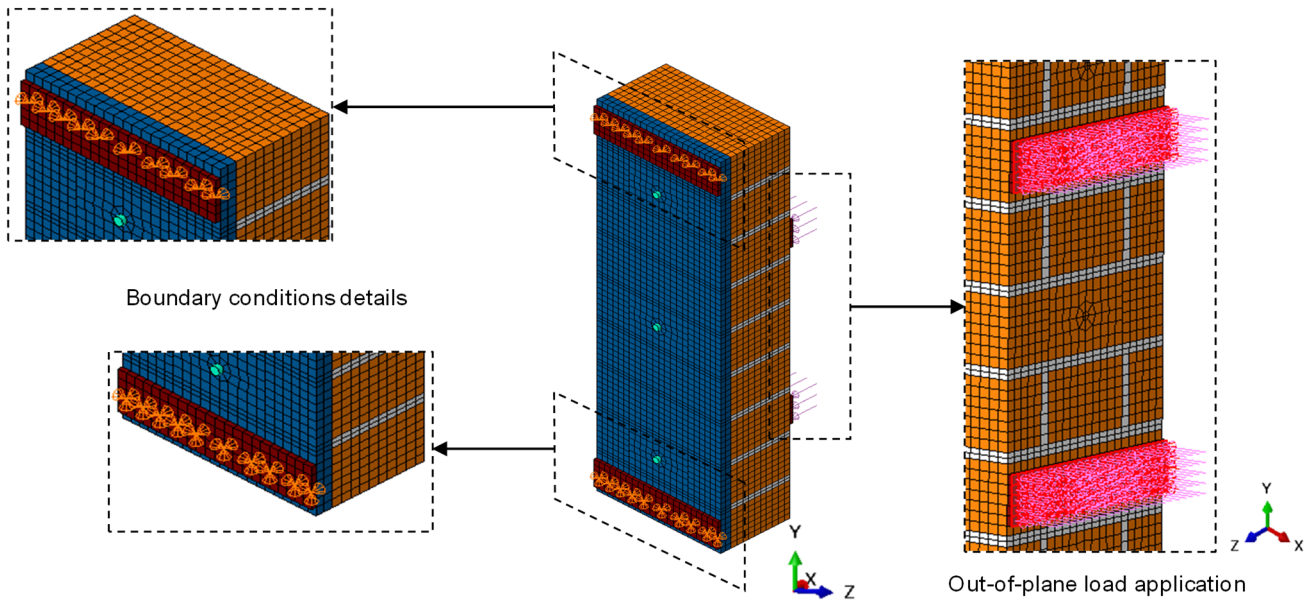


Figure 7. Numerical modelling of the masonry prisms (MP).

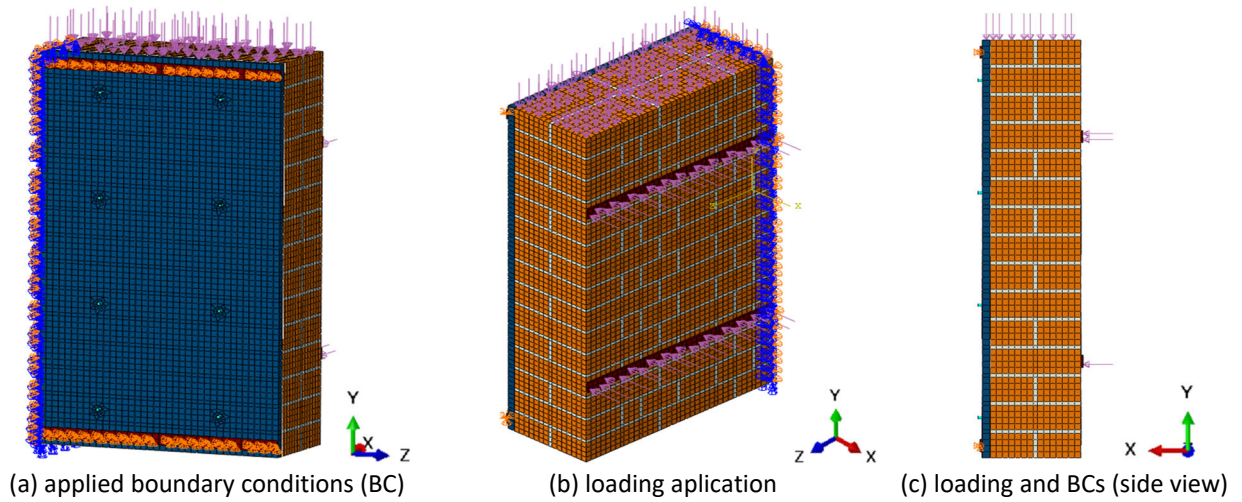


Figure 8. Numerical FE model for the study of the masonry walls (1SRW1115-NM is shown as an example).

3.4 Mechanical properties for model components

Material nonlinearity was considered for both the masonry components and the OSB panel through the so-called concrete damage plasticity (CDP) model (available in ABAQUS [41]). A non-linear behaviour was simulated for both the tension and compression regimes. An exponential softening was provided for the tension response. In compression, a hardening branch was assumed to be the post-peak response described by a parabolic softening law. These curves are represented in Figure 9 together with the corresponding parameters required as input. Note that the input for the CDP model in ABAQUS needs to be regularized aiming to guarantee mesh objectivity of the results. Therefore, the fracture energy of the curves was normalized by the mesh characteristic length h . Since the mesh is a structured one with solid FEs (see section 3.1) with an approximate mesh size of 10mm, the value of h was 10mm. The only exception is the bed mortar joints, in which $h=5\text{mm}$, and the vicinity of anchor walls in which $h=3\text{mm}$ [41,48,49].

A scalar-based damage model, coupled with the CDP plasticity model, was assumed to describe damage due to cracking (tension) and crushing (compression). The CDP model assumes a non-associated flow rule given as a Drucker-Prager hyperbolic function and requires the definition of several physically based parameters. In this regard, it was assumed: a dilation angle of $\Psi = 34$ degrees; an eccentricity parameter $e = 0.1$; a ratio between the bidirectional and unidirectional compressive strengths of masonry of $f_{b0}/f_{co} = 1.16$; a stress ratio in the tensile meridian of $k = 0.67$; and a value for the viscosity parameter of 10^{-5} . These values have been used for both the masonry components and OSB timber panel.

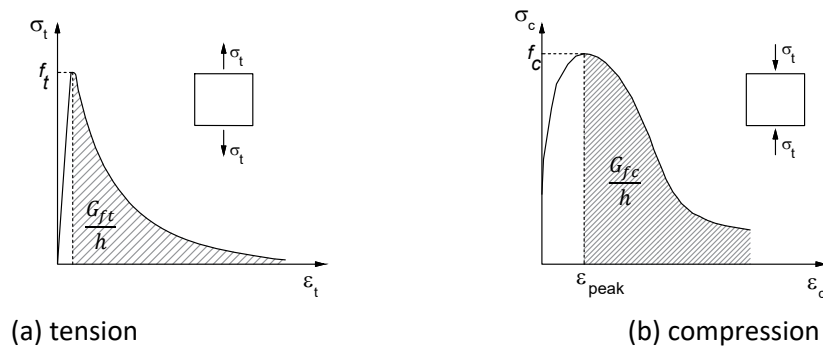


Figure 9. Assumed material nonlinear behaviour for brick units, mortar joints, and OSB panel (in which h is the mesh characteristic length).

Experimental data allowed to obtain Information for both masonry components and on its elastic properties, such as Young's modulus, but also its inelastic parameters, such as the compressive strength values [42,43]. Literature recommendations were followed to determine fracture energy values. Brick units' compressive fracture energy ($G_{fc,b}$) was defined from the recommendation given in [26]; which take into account the Model Code 90 [50]. Therefore, since brick units have a compressive strength higher than 80N/mm^2 , an average ductility index in compression of $d_{u,c} = 0.33\text{mm}$ was used. This index is the ratio between the strength and fracture energy and allowed to find a $G_{fc,b} = 29.01\text{ N/mm}$. A value within the same order of range is obtained if one uses the expression proposed in [51]. Following the same procedure, the ductility index in tension was defined to be $d_{u,t} = 0.018\text{ mm}$ [23][26], which allowed obtaining a tension fracture energy for the brick of $G_{ft,b} = 0.11\text{ N/mm}$. Although the compressive strength of mortar joints was obtained from experiments [42,43], its tensile strength was found through calibration considering the experimental data of the non-strengthened small-scale test of the masonry prisms (plain model MP00-NM). The corresponding fracture energy in tension has been defined as $G_{ft,m} = 0.02\text{ N/mm}$. This value is within the acceptable range given in [52] and allows bypassing numerical convergence issues.

To what concerns the OSB panel, its elastic properties were obtained from manufacturer specifications [52] and its compressive strength from the literature [13]. Stress and strain constitutive relations follow the same laws given in Figure 9 [13], being the fracture energy terms and the tensile strength calibrated. This calibration was conducted considering the experimental load-displacement envelope from the four-point bending test on the strengthened MPs (MPOSB-NM). It is important to address that this step was processed after the material input for both the masonry components was known through the calibration with the data from the plain model MP00-NM. The adopted material properties are given in Table 1. A linear elastic material was assumed for the anchor connectors since the observed experimental failure of the small-scale tests (used for the calibration) occurred on the masonry or OSB timber panel.

Table 1. Material properties adopted for the study.

Model component	Mass density (γ) kg/m ³	Young modulus (E) N/mm ²	Poisson ratio (μ)	Compressive strength (f_c) N/mm ²	Compressive fracture energy (G_{fc}) N/mm	Tensile strength (f_t) N/mm ²	Tensile fracture energy (G_{ft}) N/mm
Brick unit	2200	32470	0.26	87.91	29.01	5.93	0.11
Mortar joint	2170	19850	0.20	7.10	1.90	0.23	0.02
OSB panel	650.0	3500	0.24	6.60	0.86	1.85	0.32
Anchors	7850	210000	0.30	Assumed to be linear elastic			

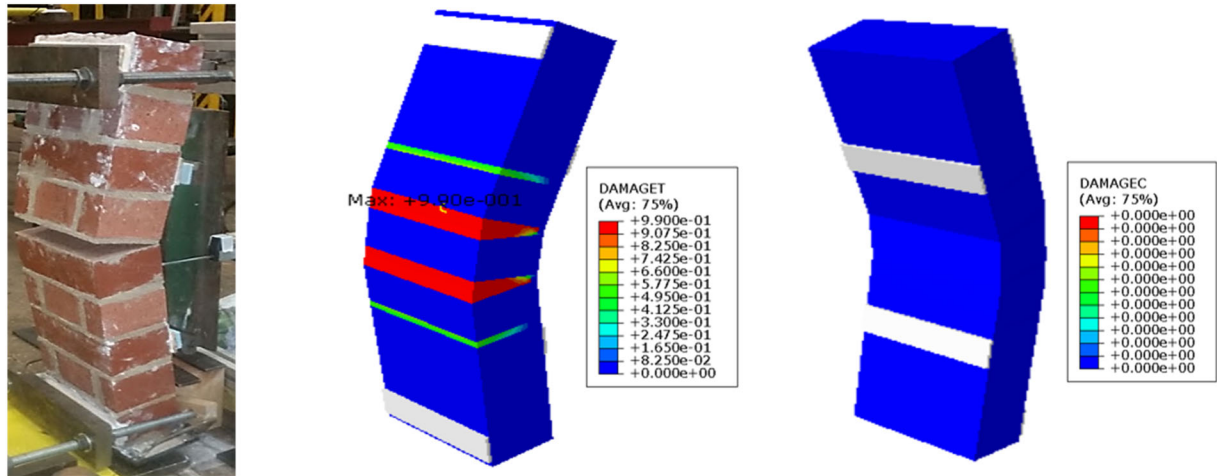
4 RESULTS AND DISCUSSION

4.1 Small-scale case study: masonry prism (MP)

4.1.1 Non-retrofitted masonry prism

The comparison between the numerical and experimental results is given here for the non-retrofitted masonry prism. Figure 10b shows that failure occurred in bed joints within the inner bearing (i.e., loading span) of the specimen. In the actual test, the total failure occurred in one bed joint since it constitutes the weakest mortar joint (Figure 10a). Yet, the numerical model exhibited a failure in two symmetrical bed joints (Figure 10b). This is expected as spatial variability of properties explained by the intrinsic material variability, differences during the construction and geometry of blocks, etc. were disregarded in the numerical model. Although, failure occurs at the same instant for both mortar joints within the inner bearing, but the amount of damage is

maximum in the upper bed joint as shown in Figure 10b. A bifurcation is found with a symmetric and an asymmetric solution when the self-weight of the model is ignored in the analysis. Furthermore, Figure 10c indicates that damage in compression due to brick units crushing is inexistent. These observations are in good agreement with the ones observed in the experimental failure patterns with the mortar joint failed in tension.



(a) observed experimental failure (b) numerical damage in tension (c) numerical damage in compression

Figure 10. Non-retrofitted masonry prism.

Figure 11 presents the numerical and experimental load-displacement curves for plain MP. The comparison shows that the numerical model predicts well the behaviour of the two specimens. The peak load occurs for negligible levels of displacement associated with high stiffness values of the composite as observed during the test. The softening branch of the curve is also in good agreement with the experimental data, being the numerical model able to capture the experimental curves. The peak load, corresponding displacement at failure, and the toughness (i.e., the area under the load-displacement curve which defines the energy absorbed) of the specimens were predicted within less than 5% difference with the average experimental results (see Table 2).

Table 2. Comparison of model and test average results for non-retrofitted masonry prism.

	Test average	Model	Relative difference (%)
Peak Load (N)	2860	2800	2.1
Displacement at Peak Load (mm)	0.058	0.055	5.0
Toughness (N.mm)	1050	1040	1.0

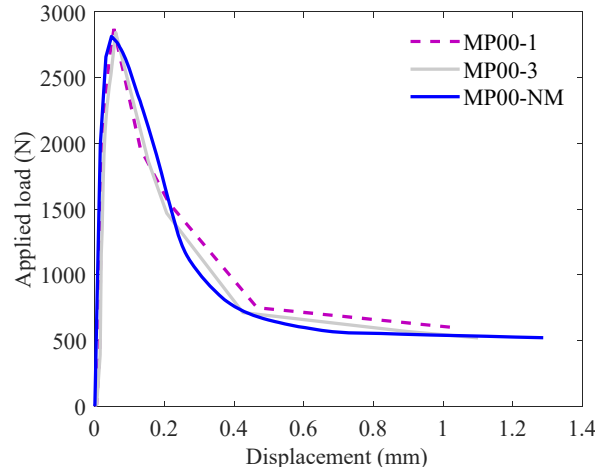


Figure 11. Comparison between the experimental and numerical load-displacement curves.

4.1.2 Retrofitted masonry prism

The quasi-static analysis performed on the retrofitted masonry prism, designated as MPOSB-NM, shows that the failure started in the bed joint within the inner bearing before propagating to the OSB timber. This failure pattern is like the one observed during the experimental tests. The failure plot in tension (DAMAGET) for a load of 5340N, which corresponds to the average load where one of the joints has failed during testing, is presented in Figure 12a. Figure 12a demonstrates that mortar joints located at the central band have failed. Still, the OSB panel shows no evidence of damage nearby the central region of the beam; at least for this level of deformation (around 1.42 mm). The numerical model indicates that the application of the OSB timber panel at the back of the MP significantly increased the capacity for out-of-plane loading. The obtained numerical damage compared with the experimental one in Figure 12c proves that the calibration has been performed successfully for the retrofitted case as well since the damage pattern corresponds to one found in all three tested specimens.

Furthermore, load vs out-of-plane displacement for the model was plotted and compared to the envelope of experimental results for six different specimens in Figure 13. A similar numerical load-displacement profile was obtained for the model. The curve shows the behaviour of the specimen at the initial elastic phase where the OSB and the masonry are bonded together before the crack was initiated at an average load of 3640N for the tested specimen and 3840N (5% variation) for the numerical model. This phase is then followed by the complete failure of the joint in the masonry prism at an average load of 7980N and 8360N (4% variation) for the tested and numerical specimen, respectively. The final phase of the curve i.e., after the applied load is more than 8360N presents a region where the masonry part has failed and the OSB is taking the load up to the failure of the OSB. The toughness at different phases, maximum load, and corresponding displacement are within less than 5% of the average test results (Table 3).

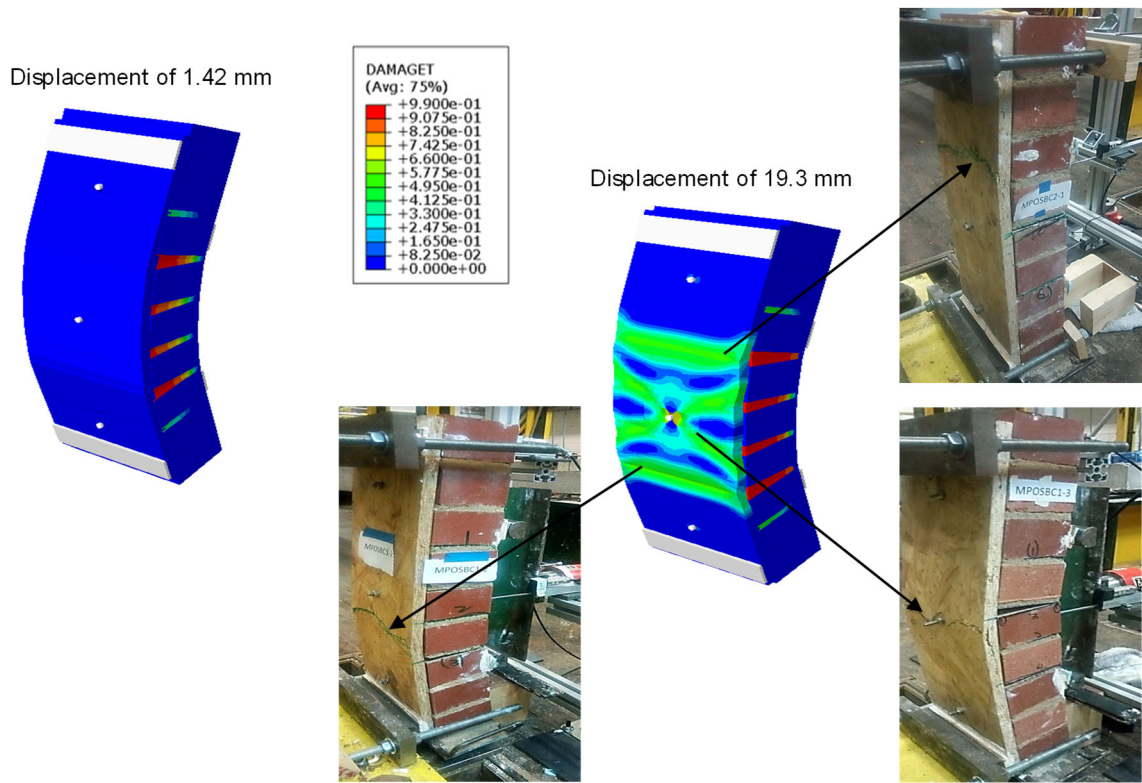


Figure 12. Retrofitted masonry prism: numerical damage in tension (DAMAGET) for a displacement of 1.42mm and 19.3mm and comparison with the observed experimental failure.

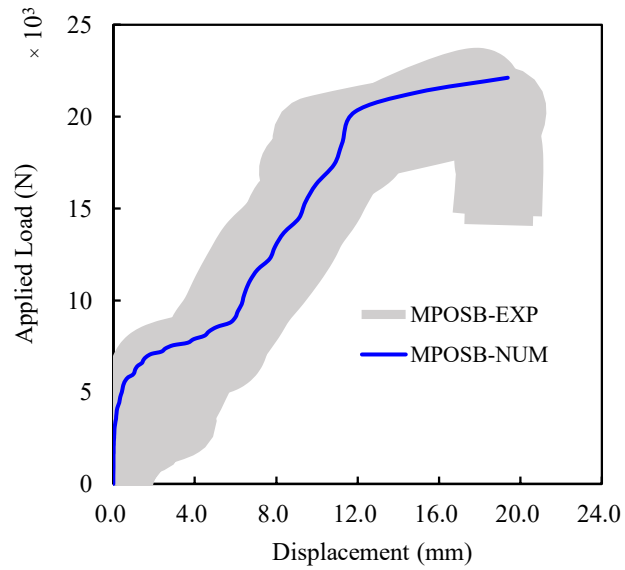


Figure 13. Experimental and numerical load-displacement curves for the retrofitted MP.

Table 3. Comparison of model and test average results for retrofitted masonry prism.

	Test average	Model	Relative difference (%)
Peak Load (N)	21100	22100	4.5
Displacement at Peak Load (mm)	18.7	19.4	3.6
Toughness (N.mm)	257000	271000	5.0

4.2 Larger-scale case study: masonry wall (MW)

4.2.1 Non-retrofitted masonry wall

The numerical results found for the plain wall show again a good agreement with the experimental data both in terms of capacity and damage (Figure 14 and Figure 15). Figure 14 shows the obtained numerical damage together with the expected failure mode. The comparison indicates that failure surfaces due to vertical bending appeared in two-bed joints (ultimately a single crack at the top part of the specimen, given the variation of normal stress due to the self-weight of the wall). Failure in the test specimen (Figure 14a) crossed the perpendicular joint due to a weaker zone, due to the spatial variability of material properties of joints. Such variability was disregarded in the numerical model and, therefore, damage in tension is maximum in one bed joint only (one failure surface) and is coherent with the experimental failure position.

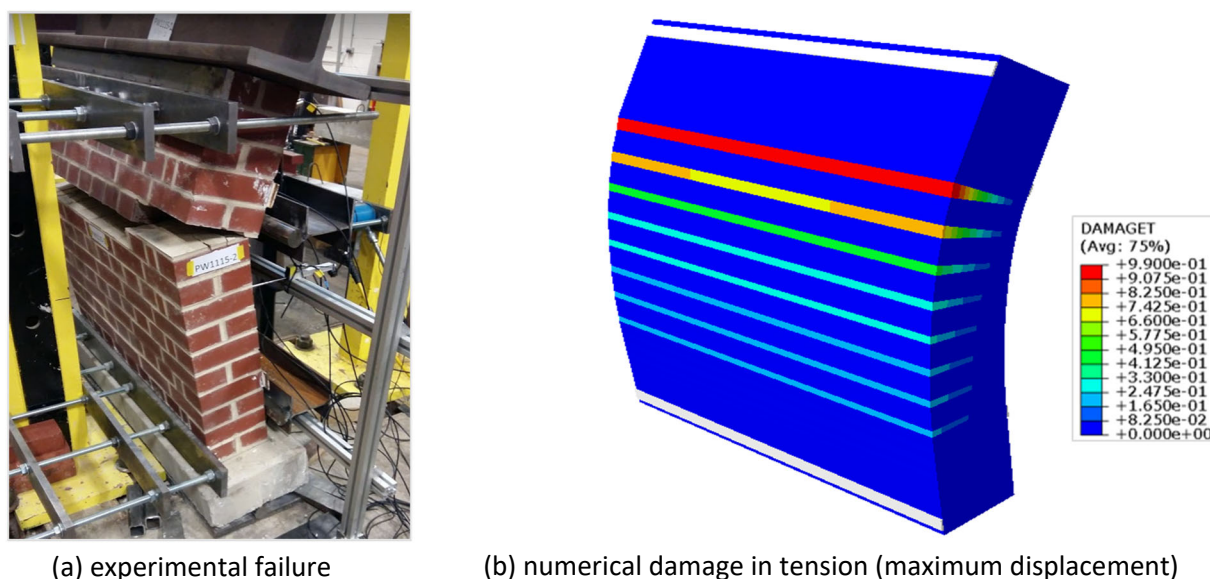


Figure 14. Non-retrofitted masonry wall.

The load-displacement curves obtained from both the experimental test and numerical analysis are given in Figure 15. The toughness, load capacity and corresponding displacement at peak load found are within a margin of 4% concerning the average experimental results (Table 4). Although a variation in the test exists in the out-of-plane displacement for a load higher than 24000N (Figure 15), with a sharp reduction of stiffness, this may be explained by the movement of the wall during the testing at the onset of cracking. This behaviour is attributed to the difficulty in the stability of the specimen during the experiment when the walls begin to damage. It was noted that it is due to the specific test arrangements where the specimen wall was placed on a cylindrical roller to prevent the arching effect. The axis of the roller was placed parallel to the face of the specimen to allow it to freely rotate around its base while deflecting out-of-plane and prevent restrained end conditions. However, since the numerical model assumed a perfect arrangement, the response is not captured and will be ignored. This behaviour was noticed and reported during the experimental campaign (see [12], [20], and [22]). Again, it is worth noticing that observations about the post-peak behaviour cannot be made during the tests because the loading was stopped after the failure of specimens. This was to avoid the total collapse of the walls and damage to the instruments.

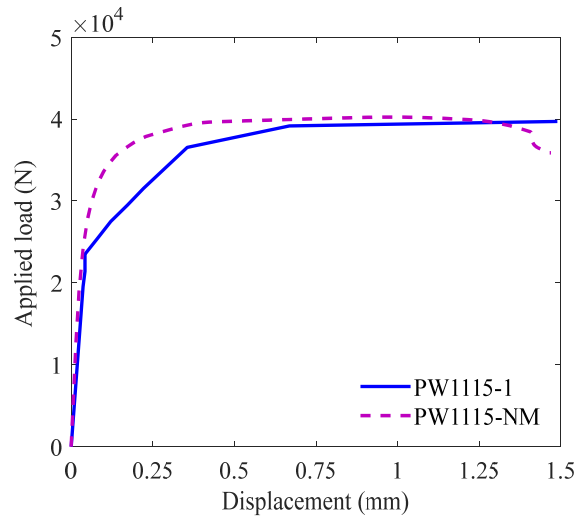


Figure 15. Experimental and numerical load-displacement curves for the plain masonry wall.

Table 4. Comparison of model and test average results (PW).

	Test average	Model	Relative difference (%)
Peak Load (N)	39000	40200	3.0
Displacement at Peak Load (mm)	1.50	1.45	3.4
Toughness (N.mm)	54800	56000	2.1

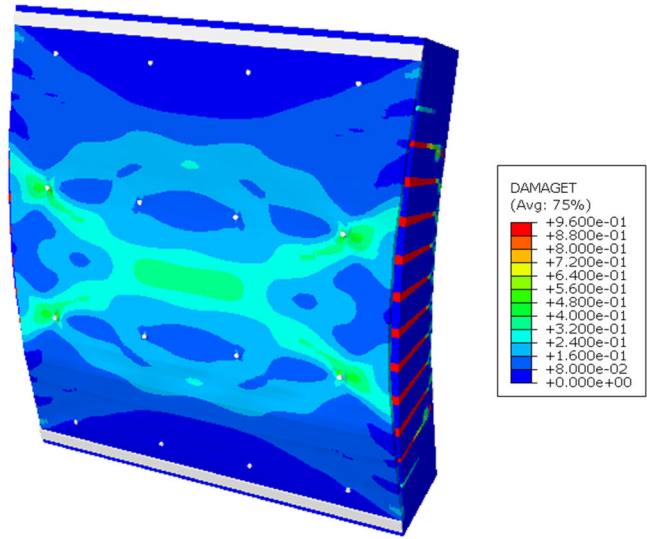
4.2.2 Single-sided retrofitted masonry wall

The numerical failure of the single-sided retrofitted (1SRW) model was compared with the damaged specimen from the test given in Figure 16. The damage pattern shows that the OSB panel fails after the mortar bed joints have reached its strength. Likewise, the load-displacement curves were compared in Figure 17. The maximum load and the corresponding displacement of the numerical model are in good agreement with the experimental results. The difference in the peak load is within 2% with the average test results as shown in Table 5. However, the difference in the out-of-plane displacement, between the test and the numerical model, is about 8.3% which can be considered a very good approximation from an engineering standpoint. Some differences are found in terms of displacement levels and can be seen in the load-displacement curve of Figure 17. The latter is attributed to the difficulty in the stability of the specimen during the experiment when the walls begin to damage. This can be ascertained from the fact that the curves compared well up to around 50000 N load, which is where the specimen failure started.

Another important observation is that the experimental curves have a clear set of steps, owing to the sequential failure of the bed joints and subsequent redistribution of the load to the OSB up to its failure. This is much less pronounced in the numerical (NM) curve. This is because the failure of the bed joints is concurrent except for the joints above the middle of the wall span which has failed at an average load of 52800N and 48600N (8% variation) for test and numerical model. Load redistribution is not obvious in the model because of the equal joint behaviour and perfect anchoring, which is not possible in the test due to the possible variation in the mortar joint during construction and minimum slack at the anchors.



(a) experimental failure



(b) numerical damage in tension (maximum displacement)

Figure 16. Retrofitted masonry wall (1SRW115-NM).

Table 5. Comparison of model and test average results (1SRW).

	Test average	Model	Relative difference (%)
Peak Load (N)	115000	116000	1.0
Displacement at Peak (mm)	20.8	17.3	8.4
Toughness (N.mm)	1940000	1750000	9.9

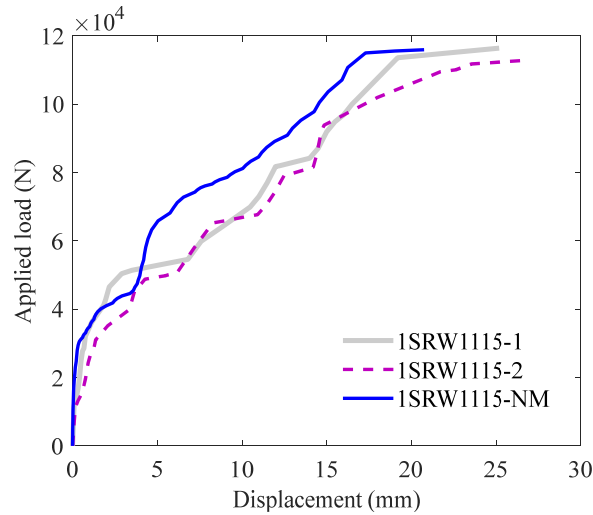


Figure 17. The experimental and numerical load-displacement curves for single-sided retrofitted wall.

4.2.3 Two-sided retrofitted masonry wall

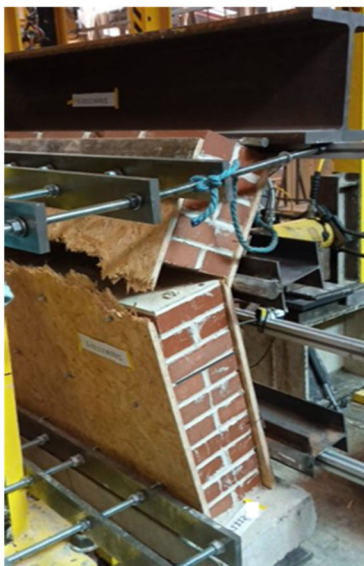
The observed failure pattern for both the numerical and experimental specimens (as shown in Figure 18) is in good agreement. The damage pattern indicates that the OSB panel in the tension side (at the back of the specimen) failed after the mortar joint has failed. The location at which the OSB failed is like what was observed in the test, in which tensile stresses spread across the middle of the panel. The OSB panel located in

the compression face had no damage as seen in the experimental results. The damage is shown for the OSB on the compression side (i.e., loading face) in Figure 18a only occurred after the failure and, therefore, not replicated in the model.

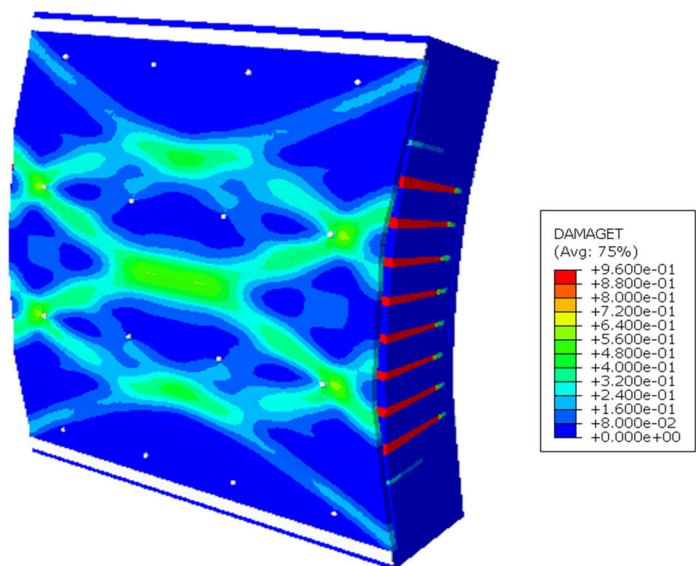
In addition to the comparison of the damage plots, the load-displacement curves for both the experimental and numerical models are presented in Figure 19. Differences between the numerical (NM) and experimental curves are especially clear after the onset of cracking, i.e., for an applied load higher than 65000N. It may be remarked that some displacement jumps are found for the experimental data, which are attributed to the stability issue of the specimen, that occur after bed joints failure during the testing. The difference in the maximum load and corresponding displacement of the numerical model and the experimental results is also within less than 10% of the average test results in Table 6.

Table 6. Comparison of model and test average results (2SRW).

	Test average	Model	Relative difference (%)
Peak Load (N)	121000	123000	1.8
Displacement at Peak Load (mm)	8.25	7.45	9.3
Toughness (N.mm)	1200000	1120000	6.7



(a) experimental failure



(b) numerical damage in tension (maximum displacement)

Figure 18. Retrofitted masonry wall (2SRW1115-NM).

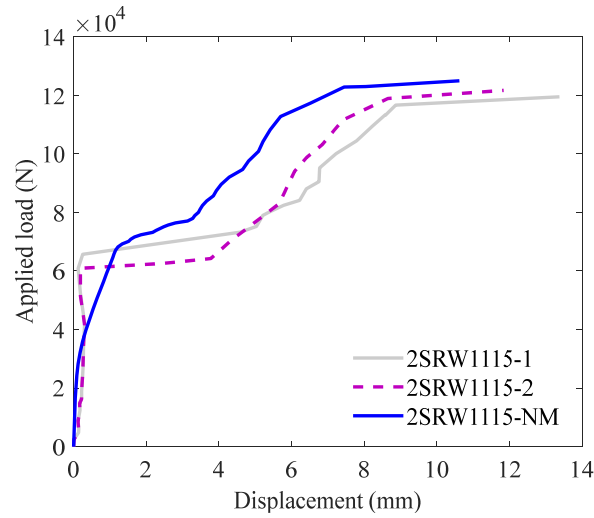


Figure 19. The experimental and numerical load-displacement curves for two-sided retrofitted masonry (2SRW1115) wall.

5 PARAMETRIC ANALYSIS

This section presents a parametric study that was developed considering the larger scale retrofitted masonry wall described in section 2. The numerical model with calibrated properties has been used to investigate three variables: (i) the position of the OSB application concerning the masonry; (ii) the thickness of the OSB panel; and (iii) the number of connectors and their spacing. A total of nine models were developed and compared as shown in Table 7. The following results were gathered for each analysis: the load capacity, the peak, and ultimate displacement, and toughness. These are taken as representative parameters aiming to compare the responses.

Table 7. Definition of the conducted parametric study.

Group	Model nomenclature	Parameter	Constant parameter
1	1SRW-18-T-16A	The side in which OSB is applied	OSB panel with 18mm of thickness together with a total of 16 anchors with $\varnothing 8\text{mm}/\text{L}50\text{mm}$ (diameter/length)
2	1SRW-10-T-16A	The thickness of the OSB panel	OSB panels applied on the tensile face of the masonry together with 16 anchors
3	1SRW-18-T-6A	The number of connectors	OSB panel with 18mm of thickness applied on the tensile face of the masonry

Nomenclature:

1SRW-18-T-16A – An OSB panel of 18mm applied on the tensile side of the masonry through 16 anchors;

1SRW-18-‘-16A – Missing letter can be a ‘C’ ‘C’ or ‘T’ depending on if the OSB panel is applied on the Compression or Tensile side, respectively. If ‘B’, the OSB panel is applied on both sides of the masonry wall.

The toughness (i.e., energy absorbed) of the specimens is estimated from the load-displacement curve using the method based on ASTM 1609. This toughness is estimated as the overall (i.e., the total area under the load-displacement curve) and the limiting toughness. The limiting toughness is the area under the curve up to a limited displacement of span/250 (BSI, 1996). This is done to understand the toughness gained due to the retrofit application when undergoing an acceptable displacement without adverse effects. Since masonry specimens deflected excessively until the failure of the OSB panel, one may address that it may contradict the BSI 1996 recommendation: “Masonry walls subjected to lateral loads shall not deflect adversely under such

loads". Such excessive deflection is, therefore, unacceptable within a structural design project, at least for new masonry structures, as it can cause visual distress to the building users (serviceability limit states) and lead to damage of other building parts. Thus, it is considered that the limiting toughness estimates the improvement due to the application of the OSB retrofit within an acceptable range.

5.1 Influence of the application position of the retrofit

To have a better understanding of how the application of the proposed OSB timber retrofit technique influences the behaviour of the masonry wall, three possible positions were investigated. The numerical analyses carried out demonstrated that the application of the OSB panel on the compression side only (1SRW-18-C-16A) results in the poorest performance, as expected. The application on the tensile side only (1SRW-18-T-16A) or on both sides (1SRW-18-B-16A) improved the out-of-plane capacity of the wall significantly. However, the 1SRW solution leads to a lower out-of-plane displacement capacity when compared to the 2SRW.

Figure 20 depicts the obtained damage plot for the numerical analyses. In general, it can be addressed that the failure mode of masonry is kept constant despite the application of the OSB panel retrofit. Differences are especially clear by analysing the obtained numerical capacity curves. Figure 21 presents the load-displacement curve for the three models and a comparative chart on the effectiveness of each application. The analysis reveals that the OSB application on the compression side of the wall only does not improve the load capacity of the wall. Nevertheless, it shows a significant increase in the toughness of the retrofitted wall (15 times higher than PW) when the allowable limit for the out-of-plane displacement of the wall is considered. Meanwhile, the application on the tensile side only shows an increment in the load capacity (2.9 times higher than PW), limiting toughness (18.6 times higher than PW), and overall toughness (31.3 times higher than PW), as shown in Figure 21.

It may be highlighted that both the 1SRW-T and 2SRW-B solutions show a similar value in terms of load capacity. The 2SRW-B solution shows a better limiting toughness than the 1SRW-T (about 1.5 times that of 1SRW-T). This observation reveals that the double side application has more limiting toughness and lesser overall toughness than the single-sided application. Therefore, the double-sided application is more resilient in the allowable range and is thus recommended for seismic applications.

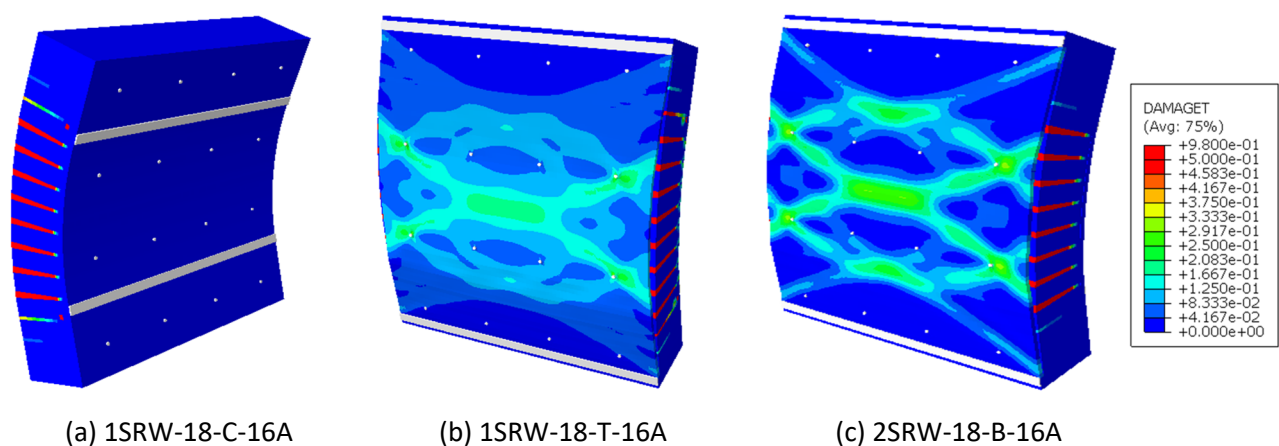
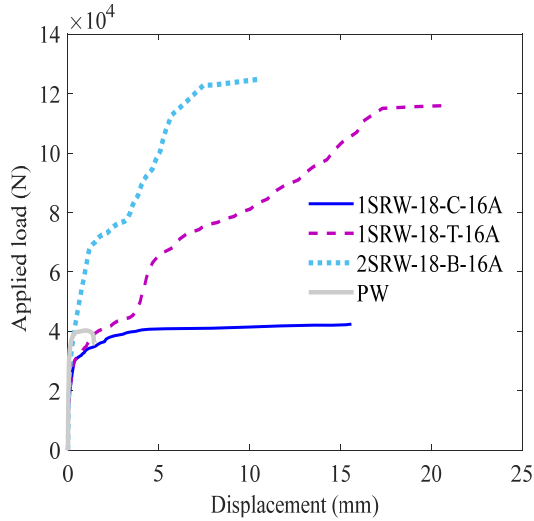
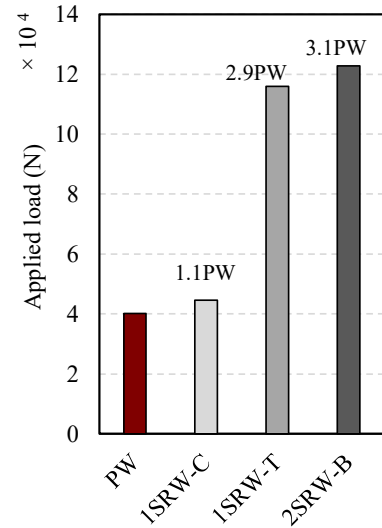


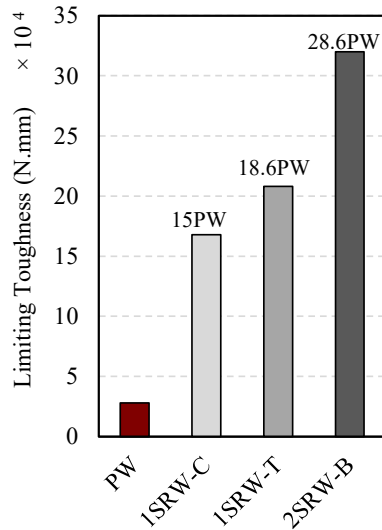
Figure 20. Damage plot for different applications of the proposed retrofit technique.



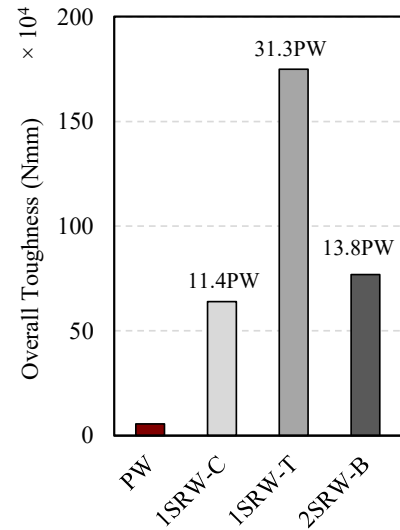
(a) load-displacement curve



(b) load capacity



(c) limiting toughness



(d) overall toughness

Figure 21. Comparison of the results found for different applications of the proposed retrofit technique.

5.2 Influence of the OSB thickness

For this study, three different values for the OSB panel thickness were examined and are given as 10mm, 18mm, and 25mm. Figure 22 presents the damage plot and Figure 23 presents the performance evaluation of each OSB thickness in terms of load capacity, limiting, and overall toughness. From the analysis, a thickness of 18mm appears to be most adequate for a retrofit application in typical masonry brick walls with 215 mm thickness. In the model with 10mm thickness, the damage plot indicates some non-uniform stress in the timber and the lowest load resistance increment. The 10mm thickness might be considered thinner for load-bearing applications because of the warping effect. Meanwhile, application with 25mm thickness shows the highest load increment (4.2 x PW), but damages appeared in the brick before the OSB is damaged as shown in the results of Figure 22. This might be too conservative because damage to the brick will only occur after the wall has lost all its integrity.

The toughness of the panels, i.e., the energy absorption capacity by the different OSB thicknesses, were evaluated within the allowable limit and the overall performance. The analysis revealed that the energy absorption capacity of the wall within the allowable limit thickness is independent of the thickness of the OSB panel. However, the overall energy capacity of the retrofitted system increases with the increase of the OSB thickness. Meanwhile, the overall toughness of the 18mm and 25mm OSB is relatively equal, even though the 25mm OSB carried more load at the expense of excessive damage to the masonry part as highlighted earlier. An inference from the latter is that an 18mm thick OSB is recommended to provide an adequate increment of load capacity (2.9 times PW), limiting toughness (6.23 times PW), and overall toughness (31.3 times PW).

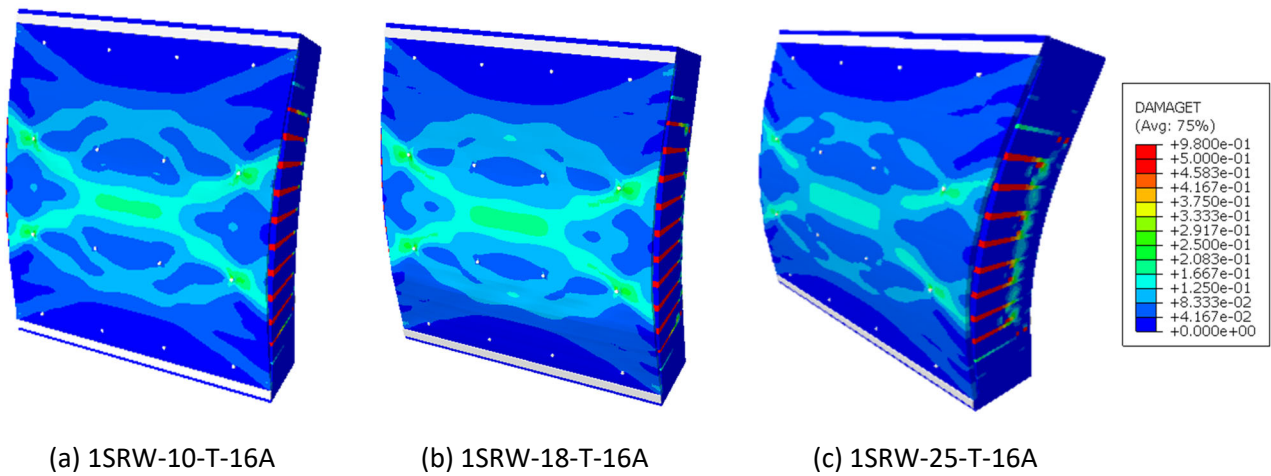
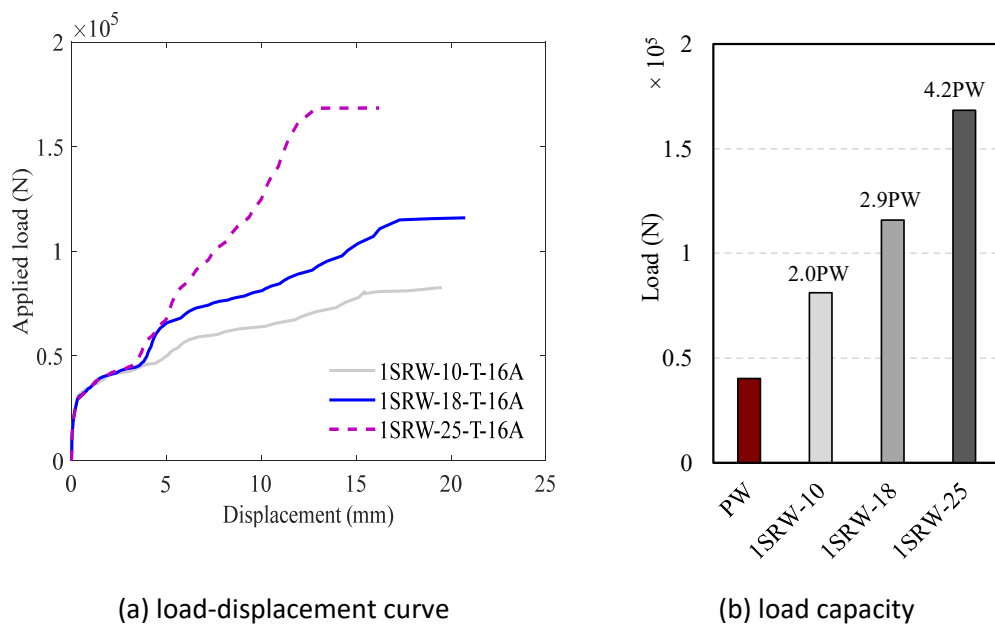


Figure 22. Damage plot for the OSB panels with different thickness values.



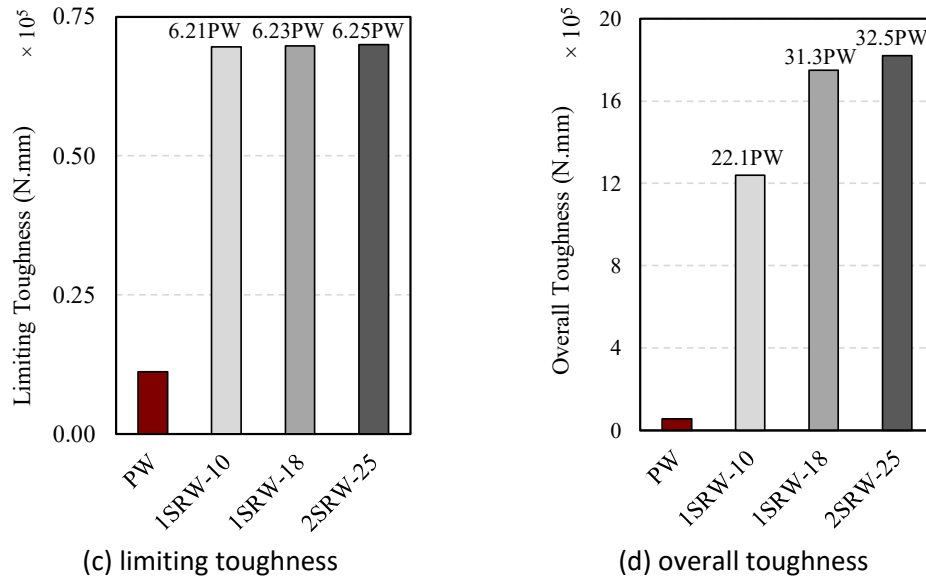


Figure 23. Comparison of the results found for OSB panels with different thickness values (located at the bottom surface of the masonry panel).

5.3 Influence of the number of connections

A proper edge distance and spacing between connectors is paramount to the performance of this proposed retrofit technique again in masonry brick walls with 215 mm thickness. The parametric analysis examined the performance of using 6, 12, and 18 anchors, to which correspond a spacing of 700/450, 280/450mm, 280/300mm (horizontal/vertical spacing). Figure 24 and Figure 25 present the damage plots and the performance evaluation charts, respectively. The analysis revealed that spacing above 500mm can reduce the effectiveness of this technique. For the 1SRW-18-T-6A, in which only six anchors were used (i.e., spacing higher than 500mm), the behaviour shows that there is not enough composite action between the masonry and the OSB timber. Hence a maximum spacing of 450mm is recommended for this application. Indeed, in the other two cases (12A and 16A), the OSB panel was able to increase the load capacity of the wall by a factor of three. Also, it is important to avoid spacings lower than 250mm to preclude close arrangements that reduce the influence cone of anchors which leads to spalling damage and thus reduces the performance.

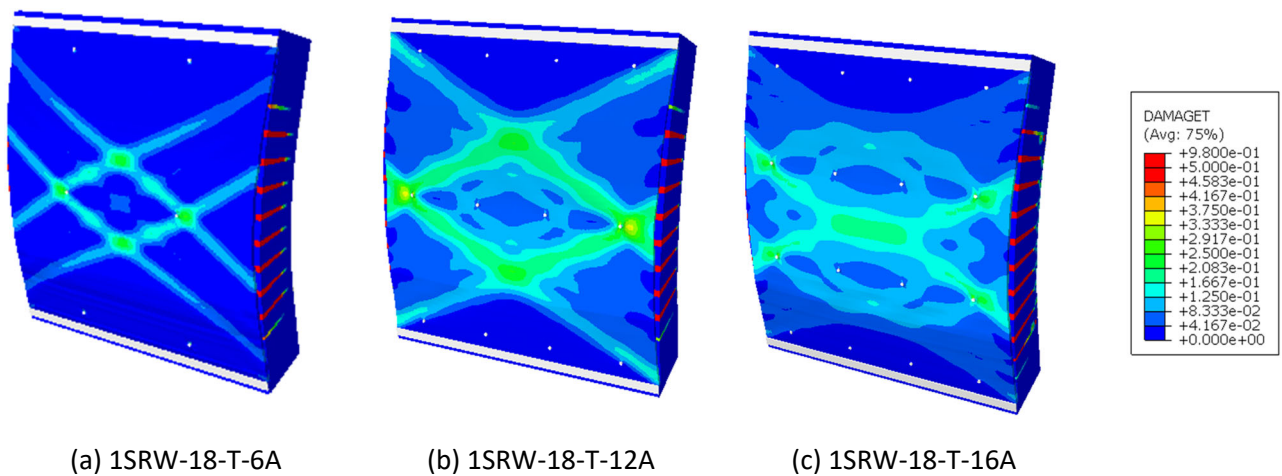


Figure 24. Damage plot for the different number of anchor connections.

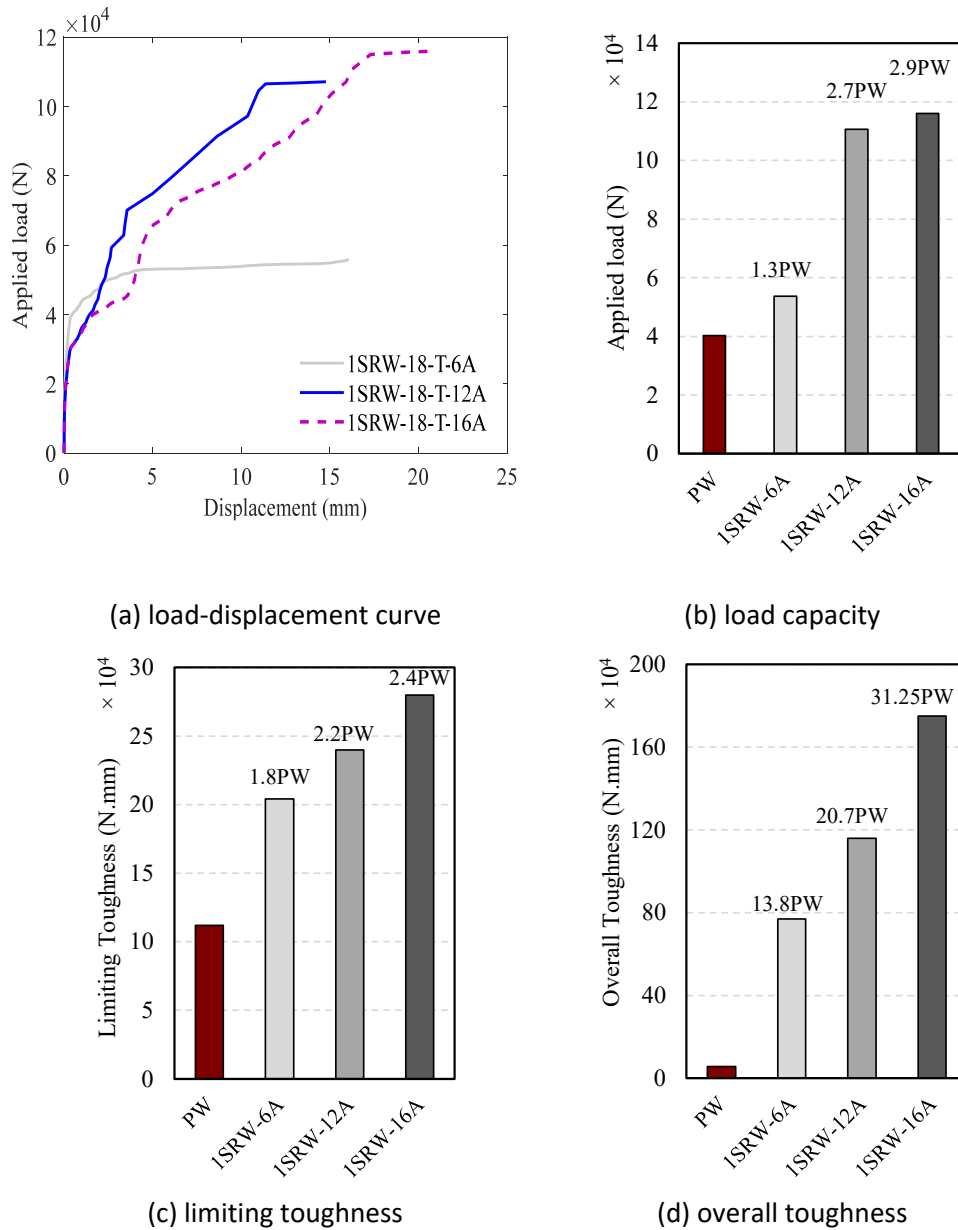


Figure 25. Comparison of the results found for OSB panels with a different number of connection anchors.

Although the load increment is higher when twelve (12A) and sixteen (16A) anchors were used, the relative difference between the latter solutions is almost residual (2.7PW and 2.9PW, respectively). The overall toughness gained when 16 anchors were used is 1.5times the toughness gained when the system applied with 12 anchors. The additional toughness gained is due to the rigidity of the composite system because of the additional 4 anchors. However, the limiting toughness of both applications (1SRW-18-T-12A and 1SRW-18-T-16A) is similar, about 2.2times that of the PW. Meanwhile, the 1SRW-18-T-6A shows the least increment in both the limiting and overall toughness of the system, which is because due to the lack of composite action between the masonry and the OSB timber with 6 anchors.

5.4 Cost evaluation of the proposed retrofit technique

This section presents a brief cost analysis of the different studied solutions for the application of OSB retrofitting. The total cost of applying the selected three thickness of the OSB was evaluated and compared

against the overall toughness gained per total cost in Table 8. After that, the cost implication based on the number of anchors used is also presented in Table 9. The costing (material and labour) is carried out using market prices in England. The labour cost is added to the cost of the anchor. Table 8 reveals that the overall toughness gained per total cost of the application is at highest when 18mm thick OSB is used. This cost analysis further substantiated the claim that the 18mm thick OSB is the most suitable solution for this type of retrofitting application. This is the most cost-effective OSB panel, and it brings a substantial gain in the load capacity and toughness of the retrofitted wall.

Similarly, the cost analysis provided in Table 9 reveals that the overall toughness gained per total cost of the application is maximum when 16 anchors are applied. This means that maximum spacing of 300mm is recommended to get the most cost-effective solution. This will ensure an adequate composite action between the masonry and the applied OSB panel. However, in cases where considerable toughness increment is not required when designing, for instance, within a displacement-based approach, the connection spacing can be increased. The latter is valid only if the maximum recommended spacing value of 500mm is ensured to guarantee the development of adequate composite action. In such a context, the total cost of applying typical fibre-based retrofit applications on one side of a 1m² masonry wall was estimated to be £152 using the market prices in England. This estimated cost is significantly higher when compared with the total cost of applying the proposed OSB retrofit technique using an 18mm OSB panel with 300mm spacing between anchor connections on single and both sides of 1m² masonry wall which are £47 and £82, respectively.

Table 8. Cost evaluation for different OSB panels with different thicknesses and considering 16 anchors for the connection with the masonry wall.

OSB thickness	OSB cost (£)	Anchor cost (£)	Total cost (£)	Overall toughness gained × PW	Toughness gained/total cost
10	6.84	35.36	42.20	22.10	0.52
18	11.75	35.36	47.11	31.25	0.66
25	16.81	35.36	52.17	32.50	0.62

Table 9. Cost evaluation for the different number of anchors using 18mm OSB.

Anchor quantity	OSB cost (£)	Anchor cost (£)	Total cost (£)	Overall toughness gained × PW	Toughness gained/total cost
6	11.75	13.26	25.01	13.80	0.55
12	11.75	26.52	38.27	20.70	0.54
16	11.75	35.36	47.11	31.25	0.66

6 FINAL REMARKS

The use of oriented stranded board (OSB) type 3 to retrofit unreinforced masonry walls has been studied and recommendations for its application addressed. An experimental campaign aimed to evaluate the capacity and the effectiveness of the proposed timber-based retrofit technique against out-of-plane failure has been conducted and reported in [36] and [37]. These experimental tests constitute the reference data, in which the numerical analyses were performed the advanced software ABAQUS on both small-scale (665 × 215 × 102.5 mm³) masonry prisms and larger-scale (1115 × 1115 × 215 mm³) masonry walls. A detailed micro-modelling approach was employed to simulate the four-point bending tests, in which a perfect mortar-brick unit bond has been assumed (interface disregarded and the interface nodes were merged). The mechanical properties used for brick units and mortar joints have been calibrated from the data available [43] and following literature recommendations. The Concrete Damage Plasticity (CDP) model, available in ABAQUS, has been assumed to

describe the constitutive material relations for the masonry components and OSB timber panel. For the retrofitted model, the connection between the masonry and the OSB panel is achieved through anchors whose behaviour is assumed to be elastic.

Quasi-static incremental nonlinear numerical analyses were performed. Numerical failure has been captured in terms of compressive and tensile damage since the CDP model is coupled with a damage parameter-based model. The obtained capacity curves were derived and represent the relationship between the out-of-plane applied load and the maximum displacement obtained. The comparison between the numerical and experimental data confirms that the developed FE models captured with high accuracy the behaviour of both the plain and retrofitted walls, in terms of ultimate load capacity and damage failure patterns. Generally, the numerical model predicted the peak load within a 5% deviation from the corresponding average failure experimental load. The corresponding displacement at failure and toughness of the models were also predicted to within less than 10% deviation from the average test results.

Since the material properties of the FE numerical model were properly calibrated with experimental evidence, a parametric study on the larger-scale walls was employed to further investigate the performance of the proposed retrofit technique. The parametric analysis confirmed that the application of an OSB panel, solely on the compression side of the masonry wall, results in a negligible improvement of the out-of-plane capacity. The analysis revealed that the thickness of the OSB panel has a favourable outcome concerning the out-of-plane performance of the masonry wall. The increase of the OSB timber thickness improves both the out-of-plane load capacity and ultimate displacement of the system. In converse, the spacing between connectors (anchor rods) has a marginal effect when it is between 250mm and 500mm. However, a spacing larger than 500mm reduces the monolithic behaviour of the system to a point that strength is conditioned by the initial failure of the OSB panel rather than in the masonry.

A cost analysis has been also performed and demonstrated that the proposed technique is cost-effective. The retrofit cost per square meter of a masonry wall, when using an 18mm OSB panel with 300mm of spacing between anchor connections, is estimated to be £47 for 1SRW and £82 for 2SRW. Such values are lower when compared with the estimated cost of £152 for typical fibre-based retrofit applications. The latter costs (materials and labour) were evaluated under market prices found in England at the date of the publication.

At last, it should be recalled that a monotonic loading can give a good insight into the seismic response of masonry structures [53,54]. However, it is unable to track materials' stiffness degradation and to explore all the possible energy dissipation mechanisms (lower deformation levels). In this regard, the field of application of the conclusions is limited, for instance, to the retrofit of masonry infill walls aiming to cope the typical out-of-plane mechanisms witnessed at the aftermath of an earthquake [55]. This is, in fact, in hand with the study from Koutas et al. [56], in which an out-of-plane monotonic loading was used to study infill masonry walls retrofitted with textile-reinforced mortar (TRM). Aiming to extend the applicability of OSB panels, further studies need to be performed. These can provide a better insight into the response of the system when subjected to two-way out-of-plane bending, bidirectional loading (in-plane and out-of-plane simultaneously), and cyclic loading [57]. In such programs, other features may influence the response, as the strength reduction of the connection and the energy dissipation of the joint during the hysteresis cycles, as seen by [58] when analysing the use of externally bonded grids within masonry panels.

ACKNOWLEDGEMENTS

This work has been funded by Leeds Anniversary Research Scholarship and coordinated by Doctor Iuorio. The authors would like to acknowledge the school of Civil Engineering at the University of Leeds for the funding and the technicians in the George Earle Laboratory for their technical support in the experimental work.

REFERENCES

- [1] A.A. Costa, A. Arêde, A. Costa, C.S. Oliveira, Out-of-plane behaviour of existing stone masonry buildings: Experimental evaluation, *Bull. Earthq. Eng.* 10 (2012) 93–111. <https://doi.org/10.1007/s10518-011-9332-9>.
- [2] P.B. Lourenço, L.C. Silva, Computational applications in masonry structures: from the meso-scale to the super-large/super-complex, *Int. J. Multiscale Comput. Eng.* 18 (2020) 1–30. <https://doi.org/10.1615/IntJMultCompEng.2020030889>.
- [3] P.B. Lourenço, Recent advances in masonry structures: Micromodelling and homogenisation, in: *Multiscale Modeling in Solid Mechanics: Computational Approaches*, Multiscale Model. Solid Mech. Comput. Approaches. (2009) 251–294.
- [4] V. Sarhosis, J. V Lemos, G. Milani, Computational Modeling of Masonry Structures Using the Discrete Element Method, IGI-Global., 2016. <https://doi.org/10.4018/978-1-5225-0231-9>.
- [5] M. Lu, A.E. Schultz, H.K. Stolarski, Application of the arc-length method for the stability analysis of solid unreinforced masonry walls under lateral loads, *Eng. Struct.* 27 (2005) 909–919. <https://doi.org/10.1016/j.engstruct.2004.11.018>.
- [6] A.I. Dogariu, Numerical Analysis of a Steel Wire Mesh Seismic Retrofitting Techniques for Masonry Structures, *Institutul Politeh. Din Iasi. Bul. Sect. Constr. Arhit.* 0, 2015, Vol.61(3), p.29 [Peer Rev. Journal]. (2015).
- [7] L.C. Silva, P.B. Lourenço, G. Milani, Derivation of the out-of-plane behaviour of masonry through homogenization strategies: micro-scale level, *Comput. Struct.* 209 (2018) 30–43. <https://doi.org/https://doi.org/10.1016/j.compstruc.2018.08.013>.
- [8] C. Wang, V. Sarhosis, N. Nikitas, Strengthening/Retrofitting Techniques on Unreinforced Masonry Structure/Element Subjected to Seismic Loads: A Literature Review, *Open Constr. Build. Technol. J.* 12 (2018) 251–268. <https://doi.org/10.2174/1874836801812010251>.
- [9] P.G. Asteris, V. Plevris, Handbook of research on seismic assessment and rehabilitation of historic structures, 2015. <https://doi.org/10.4018/978-1-4666-8286-3>.
- [10] M.A. Elgawady, P. Lestuzzi, A review of conventional seismic retrofitting techniques for URM, 13th Int. Brick Block Mason. Conf. (2004) 1–10.
- [11] S.W. Chuang, Y. Zhuge, Seismic Retrofitting of Unreinforced Masonry Buildings – A Literature Review, *Aust. J. Struct. Eng.* 6 (2005) 25–36. <https://doi.org/10.1080/13287982.2005.11464942>.
- [12] J.A. Dauda, Numerical and Experimental Investigation of Unreinforced Masonry Wall Retrofitted with Timber Panels, University of Leeds, UK, 2020.
- [13] G. Chen, B. He, Stress-strain constitutive relation of OSB under axial loading: An experimental investigation, *BioResources.* 12 (2017) 6142–6156. <https://doi.org/10.15376/biores.12.3.6142-6156>.
- [14] B. Sustersic, I. Dujic, Seismic Strengthening of Existing Concrete and Masonry Buildings with Crosslam Timber Panels, in: S. Aicher, H.W. Reinhardt, H. Garrecht (Eds.), *Mater. Joints Timber Struct. Recent Dev. Technol.*, 2014: pp. 713–723. <https://doi.org/10.1007/978-94-007-7811-5>.
- [15] A. Borri, R. Sisti, M. Corradi, Seismic retrofit of stone walls with timber panels and steel wire ropes,

Proc. Inst. Civ. Eng. - Struct. Build. (2020) 1–14. <https://doi.org/10.1680/jstbu.19.00100>.

- [16] F. Guerrini, G. Damiani, N. Miglietta, M. Graziotti, Cyclic response of masonry piers retrofitted with timber frames and boards, *Proc. ICE - Struct. Build.* (2020) 54.
- [17] G. Vasconcelos, P.B. Lourenço, Experimental characterization of stone masonry in shear and compression, *Constr. Build. Mater.* 23 (2009) 3337–3345. <https://doi.org/10.1016/j.conbuildmat.2009.06.045>.
- [18] K. Hamoush, S. McGinley, M. Mlakar, P. Scott, D. Murray, Out-of-plane strengthening of masonry walls with reinforced composite, *J. Compos. Constr.* 5 (3) (2001) 139–145.
- [19] A. Costa, A. Arêde, A. Costa, Experimental study of the out-of-plane behaviour of unreinforced sacco stone masonry walls: Comparative analysis of two different test setups, in: 9th Int. Mason. Conf., Guimarães, 2014: pp. 1–9.
- [20] N. Ismail, J.M. Ingham, In-plane and out-of-plane testing of unreinforced masonry walls strengthened using polymer textile reinforced mortar, *Eng. Struct.* 118 (2016) 167–177. <https://doi.org/10.1016/j.engstruct.2016.03.041>.
- [21] Y. Lin, D. Lawley, L. Wotherspoon, J.M. Ingham, Out-of-plane Testing of Unreinforced Masonry Walls Strengthened Using ECC Shotcrete, *Structures*. 7 (2016) 33–42. <https://doi.org/10.1016/j.istruc.2016.04.005>.
- [22] N. Gattesco, I. Boem, Out-of-plane behavior of reinforced masonry walls: Experimental and numerical study, *Compos. Part B Eng.* 128 (2017) 39–52. <https://doi.org/10.1016/j.compositesb.2017.07.006>.
- [23] P.B. Lourenço, Computational strategies for masonry structures, 1996. [https://doi.org/ISBN 90-407-1221-2](https://doi.org/ISBN%2090-407-1221-2).
- [24] J. Asteris, P. Sarhosis, V. Mohebbkhah, A. Plevris, V. Papaloizou, L. Komodromos, P. Lemos, Numerical modelling of historic masonry structures, in: V. Asteris, P. Plevris (Ed.), *Handb. Res. Seism. Assess. Rehabil. Hist. Struct.* Pp.213–256, IGI Glob. USA.ASTM 1609, 2015: pp. 213–256.
- [25] S. Zhang, D. Yang, Y. Sheng, S.W. Garrity, L. Xu, Numerical modelling of FRP-reinforced masonry walls under in-plane seismic loading, *Constr. Build. Mater.* 134 (2017) 649–663. <https://doi.org/10.1016/j.conbuildmat.2016.12.091>.
- [26] M. Angelillo, P.B. Lourenço, G. Milani, Masonry behaviour and modelling, in: M. Angelillo (Ed.), *CISM Int. Cent. Mech. Sci. Courses Lect.*, 2014: pp. 1–26. https://doi.org/10.1007/978-3-7091-1774-3_1.
- [27] A.M. D’Altri, V. Sarhosis, G. Milani, J. Rots, S. Cattari, S. Lagomarsino, E. Sacco, A. Tralli, G. Castellazzi, S. de Miranda, Modeling Strategies for the Computational Analysis of Unreinforced Masonry Structures: Review and Classification, *Arch. Comput. Methods Eng.* (2019). <https://doi.org/10.1007/s11831-019-09351-x>.
- [28] H. Maccarini, G. Vasconcelos, H. Rodrigues, J. Ortega, P.B. Lourenço, Out-of-plane behavior of stone masonry walls: Experimental and numerical analysis, *Constr. Build. Mater.* (2018). <https://doi.org/10.1016/j.conbuildmat.2018.05.216>.
- [29] L.C. Silva, P.B. Lourenço, G. Milani, Numerical homogenization-based seismic assessment of an English-bond masonry prototype: Structural level application, *Earthq. Eng. Struct. Dyn.* 49 (2020) 841–862. <https://doi.org/10.1002/eqe.3267>.
- [30] P.B. Zucchini, A. Lourenco, A micro-mechanical model for the homogenisation of masonry, *Int. J. Solids Struct.* 39 (2002) 3233–3255.
- [31] J. Pande, G. N. Liang, J. X. Middleton, Equivalent elastic moduli for brick masonry. *Comput Geotech* 8, 243–265., *Comput. Geotech.* 8 (1989) 243–265.
- [32] A. Zucchini, P.B. Lourenço, A coupled homogenisation-damage model for masonry cracking, *Comput.*

Struct. 82 (2004) 917–929. <https://doi.org/10.1016/j.compstruc.2004.02.020>.

- [33] F. Peña, P.B. Lourenço, N. Mendes, D. V. Oliveira, Numerical models for the seismic assessment of an old masonry tower, *Eng. Struct.* 32 (2010) 1466–1478. <https://doi.org/10.1016/j.engstruct.2010.01.027>.
- [34] V. Sarhosis, T. Forgács, J. V Lemos, Macro - and micro-scale modelling of masonry structures using the Discrete Element Method, (2020) 2–5.
- [35] D.P. Abrams, O. AlShawa, P.B. Lourenço, L. Sorrentino, Out-of-Plane Seismic Response of Unreinforced Masonry Walls: Conceptual Discussion, Research Needs, and Modeling Issues, *Int. J. Archit. Herit.* 11 (2017) 22–30. <https://doi.org/10.1080/15583058.2016.1238977>.
- [36] J.A. Dauda, P. Lourenço, O. Iuorio, Out-of-Plane Testing of Masonry Walls Retrofitted with Oriented Strand Board (OSB) Timber Panels, *Proc. Inst. Civ. Eng. - Struct. Build.* (2020) 1–33. <https://doi.org/10.1680/jstbu.19.00095>.
- [37] O. Iuorio, J.A. Dauda, P.B. Lourenço, Experimental Evaluation of Out-of-Plane Strength of Masonry Walls Retrofitted with Oriented Strand Board, *Constr. Build. Mater.* (2020).
- [38] A. Anon, Brick bonds: heritage directory notes, (2009).
- [39] ASTM E518 -15, Standard Test Methods for Flexural Bond Strength of Masonry 1, *Annu. B. ASTM Stand.* (2015) 1–5. <https://doi.org/10.1520/E0518-09.2>.
- [40] ASTM E72 – 15, Standard test methods of conducting strength tests of panels for building construction, *Annu. B. ASTM Stand.* (2015).
- [41] ABAQUS, Finite Element Analysis (Theory manual). RI:Dassault Systèmes Simulia Corporation, 2014.
- [42] J.A. Dauda, O. Iuorio, P.B. Lourenço, Characterization of brick masonry: Study towards retrofitting URM walls with timber-panels, *Proc. Int. Mason. Soc. Conf. 0* (2018) 1963–1978.
- [43] J.A. Dauda, O. Iuorio, P.B. Lourenço, Numerical analysis and experimental characterisation of brick masonry, *Int. J. Mason. Res. Innov.* (2020). <https://doi.org/10.1504/IJMRI.2020.107994>.
- [44] C.R. Willis, M.C. Griffith, S.J. Lawrence, Horizontal Bending of Unreinforced Clay Brick Masonry, *Mason. Int.* 17 (2004) 109–121.
- [45] S. V. Glass, S.L. Zelinka, Moisture Relations and Physical Properties of Wood, in: C.D. Risbrudt, M.A. Ritter, Theodore H. Wegner (Eds.), *Wood Handb. Wood as an Eng. Mater.*, Centennial, United States Department of Agriculture Forest Service, Madison, Wisconsin, 2010: pp. 4–17. <https://doi.org/10.1161/01.RES.39.4.523>.
- [46] K. Park, H. Choi, G.H. Paulino, Assessment of cohesive traction-separation relationships in ABAQUS: A comparative study, *Mech. Res. Commun.* 78 (2016) 71–78. <https://doi.org/https://doi.org/10.1016/j.mechrescom.2016.09.004>.
- [47] P.B. Lourenço, D.P. Abrams, N. Mendes, A.A. Costa, A.C. Costa, Challenges in modeling out-of-plane seismic response of existing masonry buildings, *12th North Am. Mason. Conf.* (2015).
- [48] Z.P. Bažant, B.H. Oh, Crack band theory for fracture of concrete, *Matériaux Constr.* 16 (1983) 155–177. <https://doi.org/10.1007/BF02486267>.
- [49] J. Oliver, A consistent characteristic length for smeared cracking models, *Int. J. Numer. Methods Eng.* 28 (1989) 461–474. <https://doi.org/10.1002/nme.1620280214>.
- [50] CEB-FIP, Model Code 90, Thomas Telford Ltd., UK. (1993).
- [51] G. Magenes, P. Morandi, A. Penna, Test results on the behaviour of masonry under static cyclic in plane lateral loads, *Tech. Rep. ESECMaSE Work Packag. 7, Deliv. D7.1 c, Enhanc. Saf. Effic. Constr. Mason. Struct. Eur.* (2008).

- [52] H. Skovbo, OSB Technical Information, Eur. Panel Fed. (2009) 10.
- [53] K. Yasser, D. Robert, Rehabilitation of Masonry Walls Using Unobtrusive FRP Techniques for Enhanced Out-of-Plane Seismic Resistance, *J. Compos. Constr.* 10 (2006) 213–222. [https://doi.org/10.1061/\(ASCE\)1090-0268\(2006\)10:3\(213\)](https://doi.org/10.1061/(ASCE)1090-0268(2006)10:3(213)).
- [54] M.C. Griffith, J. Kashyap, M.S. Mohamed Ali, Flexural displacement response of NSM FRP retrofitted masonry walls, *Constr. Build. Mater.* 49 (2013) 1032–1040. <https://doi.org/https://doi.org/10.1016/j.conbuildmat.2012.06.065>.
- [55] H. Kaplan, H. Bilgin, S. Yilmaz, H. Binici, A. Öztas, Structural damages of L'Aquila (Italy) earthquake, *Nat. Hazards Earth Syst. Sci.* 10 (2010) 499–507.
- [56] L.N. Koutas, D.A. Bournas, Out-of-Plane Strengthening of Masonry-Infilled RC Frames with Textile-Reinforced Mortar Jackets, *J. Compos. Constr.* 23 (2019) 4018079. [https://doi.org/10.1061/\(ASCE\)CC.1943-5614.0000911](https://doi.org/10.1061/(ASCE)CC.1943-5614.0000911).
- [57] C. Papanicolaou, T. Triantafillou, M. Lekka, Externally bonded grids as strengthening and seismic retrofitting materials of masonry panels, *Constr. Build. Mater.* 25 (2011) 504–514. <https://doi.org/https://doi.org/10.1016/j.conbuildmat.2010.07.018>.
- [58] D. Riccadonna, I. Giongo, G. Schiro, E. Rizzi, M.A. Parisi, Experimental shear testing of timber-masonry dry connections for the seismic retrofit of unreinforced masonry shear walls, *Constr. Build. Mater.* 211 (2019) 52–72. <https://doi.org/https://doi.org/10.1016/j.conbuildmat.2019.03.145>.